J. Fluid Mech. (2009), *vol.* 632, *pp.* 17–48.
doi:10.1017/S0022112009006132 Printed in the United Kingdom

Measurements of molecular mixing in a high-Schmidt-number Rayleigh–Taylor mixing layer

NICHOLAS J. MUESCHKE[1], OLEG SCHILLING[2], DAVID L. YOUNGS[3] AND MALCOLM J. ANDREWS[1,4]†

[1]Department of Mechanical Engineering, Texas A&M University, College Station, TX 77843, USA
[2]Lawrence Livermore National Laboratory, Livermore, CA 94551, USA
[3]Atomic Weapons Establishment, Aldermaston, Reading, Berkshire RG7 4PR, UK
[4]Los Alamos National Laboratory, Los Alamos, NM 87545, USA

(Received 12 December 2007 and in revised form 15 January 2009)

Molecular mixing measurements are reported for a high-Schmidt-number ($Sc \sim 10^3$), small-Atwood-number ($A \approx 7.5 \times 10^{-4}$) buoyancy-driven turbulent Rayleigh–Taylor (RT) mixing layer in a water channel facility. Salt was added to the top water stream to create the desired density difference. The degree of molecular mixing was measured as a function of time by monitoring a diffusion-limited chemical reaction between the two fluid streams. The pH of each stream was modified by the addition of acid or alkali such that a local neutralization reaction occurred as the two fluids molecularly mixed. The progress of this neutralization reaction was tracked by the addition of phenolphthalein – a pH-sensitive chemical indicator – to the acidic stream. Accurately calibrated backlit optical techniques were used to measure the average concentration of the coloured chemical indicator. Comparisons of chemical product formation for pre-transitional buoyancy- and shear-driven mixing layers are given. It is also shown that experiments performed at different equivalence ratios (acid/alkali concentrations) can be combined to obtain a mathematical relationship between the coloured product formed and the density variance. This relationship was used to obtain high-fidelity quantitative measures of the degree of molecular mixing which are independent of probe resolution constraints. The dependence of molecular mixing on the Schmidt and Reynolds numbers is examined by comparing the current $Sc \sim 10^3$ measurements with previous $Sc = 0.7$ gas-phase and $Pr = 7$ (where Pr is the Prandtl number) liquid-phase measurements. This comparison indicates that the Schmidt number has a large effect on the quantity of mixed fluid at small Reynolds numbers $Re_h < 10^3$. At larger Reynolds numbers, corresponding to later times in this experiment, all mixing parameters indicated a greater degree of molecular mixing and a decreased Schmidt number dependence. Implications for the development and quantitative assessment of turbulent transport and mixing models appropriate for RT instability-induced mixing are discussed.

1. Introduction

A fundamental understanding of the physics of turbulence is crucial to the development of predictive models of turbulent mixing. Indeed, shear-driven

† Email address for correspondence: mandrews@lanl.gov

turbulence, passive scalar mixing and combustion have received extensive experimental, numerical and theoretical attention (Warhaft 2000; Veynante & Vervisch 2002; Fox 2003; Dimotakis 2005). Mixing induced purely by buoyancy-driven turbulence remains an open area of research, as such flows become complex due to the coupling of the density and velocity fields. The present study uses a novel combination of passive scalar and reacting flow experimental techniques to investigate molecular mixing dynamics in a high-Schmidt-number Rayleigh–Taylor (RT) instability-driven turbulent mixing layer with no superimposed shear.

1.1. *Overview of the Rayleigh–Taylor instability*

The RT instability occurs when a density interface is subject to a normal pressure gradient such that the pressure increases from the heavier fluid of density ρ_1 to the lighter fluid of density ρ_2 (Rayleigh 1884; Taylor 1950). A typical configuration is a heavy fluid over a light fluid in a gravitational field that forms a hydrostatic pressure gradient. At early times, when the amplitudes of the initial perturbation at the interface between the two fluids are much smaller than their respective wavelengths, such perturbations grow according to linear instability theory (Chandrasekhar 1961). The structures of rising lighter fluid are referred to as 'bubbles', and the structures of falling heavier fluid are referred to as 'spikes'. The RT instability transitions to a nonlinear growth phase when the growing bubble and spike amplitudes approach the perturbation wavelength (Youngs 1984; Haan 1989). The flow eventually becomes turbulent and grows self-similarly. In the small-Atwood-number case considered here, the fronts of the penetrating bubbles and spikes ($h_b \approx h_s \approx h/2$) grow nearly symmetrically, and the total width of the mixing layer h grows as (Anuchina *et al.* 1978; Youngs 1984)

$$\frac{h}{2} = \alpha\, Agt^2, \tag{1.1}$$

where the Atwood number $A = (\rho_1 - \rho_2)/(\rho_1 + \rho_2)$ is a dimensionless measure of the density contrast between the fluids, g is the acceleration, and α is a dimensionless growth parameter. In the present experiment a small Atwood number (7.5×10^{-4}) is considered, as larger-Atwood-number flows are more susceptible to refractive index effects (Ramaprabhu & Andrews 2003).

RT instabilities occur in a variety of physical processes and over a wide range of length and time scales. Buoyancy-driven hydrodynamic instabilities, including the RT instability, may limit the formation of heavy elements during stellar implosions (Smarr *et al.* 1981). On a smaller scale, many oceanographic and atmospheric currents are buoyancy-driven due to temperature or concentration gradients (Cui & Street 2004; Molchanov 2004). On a yet smaller scale, the breakup of fuel droplets in internal combustion engines has been related to RT instabilities (Thomas 2003; Marmottant & Villermaux 2004). At very small scales, the implosion of inertial confinement fusion (ICF) target capsules are highly susceptible to acceleration-driven instabilities, where mixing of the hot inner fuel and the cold outer shell material can limit the total energy yield (Lindl 1998; Betti *et al.* 2001; Atzeni & Meyer-ter-Vehn 2004). Buoyancy-generated turbulence provides an efficient mechanism for mixing the constituent miscible fluids (Linden & Redondo 1991). Despite the importance that molecular mixing may have in these applications, a comprehensive understanding of the buoyancy-driven mixing process, the coupled molecular mixing and the associated modelling remain an open area of research.

1.2. *Previous measurements of molecular mixing*

Quantitative measurements of molecular mixing have been reported for many classical shear-driven turbulent flows. In particular, a variety of experiments have been designed to monitor a diffusion-limited chemical reaction to quantify the degree of molecular mixing. Konrad (1977) examined gas-phase mixing in free-shear flows with a Schmidt number $Sc = \nu/D = 0.7$ (where ν is the kinematic viscosity and D is the species diffusivity). Breidenthal (1979, 1981) performed similar measurements in liquid-phase turbulent shear layers with $Sc \sim 10^3$. Both Konrad (1977) and Breidenthal (1979, 1981) quantified the degree of molecular mixing using backlit optical techniques to measure the absorption of light by a specific chemical species. A key result from these studies was an integral measure of the chemical product concentration P/δ, where P is the equivalent thickness of chemical product across the mixing layer and δ is the width (vorticity thickness) of the turbulent shear layer. It was reported that P/δ is a function of the Schmidt number, velocity ratio $r = U_1/U_2$, initial conditions and Reynolds number up to a transition range after which the mixing layer became entrainment-limited. Once the mixing layer crossed the threshold-Reynolds-number range, P/δ became independent of all parameters except the Schmidt number. For gas-phase $Sc = 0.7$ experiments, Konrad (1977) reported $P/\delta \approx 0.65$ for $Re_\delta = \Delta U\, \delta/\nu < 5000$ and $P/\delta \approx 0.81$ at higher Reynolds numbers. This contrasts with the much lower values reported for liquid-phase experiments (Breidenthal 1979, 1981), where $P/\delta = 0.05$–0.3 was measured in pre-transitional mixing layers at different velocity ratios and $P/\delta = 0.365 \pm 0.02$ at $Re_\delta > 8000$. Koochesfahani & Dimotakis (1986) extended this work using a combination of passive scalar and reacting flow techniques to quantify the amount of chemical product formed (measuring post-transition values of P/δ) and the probability density function (p.d.f.) of the high-speed fluid. The statistical composition of the mixed fluid was quantified by calculating the first moment of the interior portion of the high-speed fluid p.d.f. These results showed that the Schmidt number significantly influenced the degree of molecular mixing both before and after the mixing transition in shear flows.

Reacting flow techniques have also been used to measure mixing in turbulent jets. Shea (1977) used chemically reacting gases to measure the effects of Reynolds number and equivalence ratio on the reduction of the initial chemical reactants. Zhang, Schneider & Collicott (1995) and Zhang & Schneider (1995) used a similar liquid-phase configuration, phenolphthalein indicator and experimental methods as Breidenthal (1979, 1981) to study how variations in exit geometry affected the degree of molecular mixing in turbulent jets. Analogous to the measurement of P/δ by Konrad (1977) and Breidenthal (1979, 1981), Zhang *et al.* (1995) also quantified the degree of molecular mixing by integrating the measured-concentration chemical indicator across the span of the jet at specific downstream locations. It was concluded that the total amount of chemical product formed can be increased by modifying the jet exit geometry.

Few such measurements of molecular mixing have been reported for turbulent RT driven mixing layers. Using a water channel (Wilson & Andrews 2002; Ramaprabhu & Andrews 2004; Mueschke, Andrews & Schilling 2006) analogous to the two-stream configurations used by Konrad (1977) and Breidenthal (1979, 1981), the degree of molecular mixing was measured for a buoyancy-driven mixing layer, where one stream was heated so that $T_1 \neq T_2$, and the upper and lower stream velocities were matched. A complete description of the water channel facility is provided in § 2. In this configuration, temperature was a marker for the density and $Pr = \nu/\chi \equiv Sc = 7$, where χ is the thermal diffusivity of water. No chemical reaction was used in these

experiments; instead, a high-resolution thermocouple system measured pointwise temperatures that were related to density through an equation of state (Kukulka 1981). Mueschke *et al.* (2006) reported the time evolution of the molecular mixing parameter, θ (defined in (4.4)) along the centre plane of the mixing layer, analogous to the intensity of segregation parameter (Danckwerts 1952). Kraft, Banerjee & Andrews (2009) used hot-wire techniques to measure late-time values of θ in gas-phase experiments, using air and helium in which $Sc = 0.7$.

The water and gas channel experiments just described reported measurements for moderate species diffusivity cases of $Sc = 7$ and $Sc = 0.7$, respectively. A different set of experiments by Linden & Redondo (1991) and Linden, Redondo & Youngs (1994) considered the degree of molecular mixing in a RT mixing layer, in which the density difference was created by adding salt to the top fluid such that $Sc \sim 10^3$. In these experiments, an unstable stratification of salt water over fresh water was created when a thin barrier separating the fluids was rapidly withdrawn. Linden *et al.* (1994) used two separate measurement techniques to quantify the degree of mixing. First, electrical conductivity probes were used to measure the salt concentration pointwise. In addition, methods similar to those used by Breidenthal (1979) and Zhang *et al.* (1995) were adopted to measure the formation of coloured phenolphthalein indicator. However, the resulting product formation measurements were limited to the concentration profiles of the indicator for a single equivalence ratio (see (3.2)) and the time evolution of the centre plane indicator concentration at several equivalence ratios. The present work will also report profiles of chemical product formation; however, these results will be extended by developing a relationship between the measured product concentrations, the molecular mixing parameter θ and its global equivalent Θ, both defined in § 4.

1.3. *Present investigation*

The current work combines aspects of the reacting flow experiments of Breidenthal (1979, 1981), Linden *et al.* (1994) and Zhang *et al.* (1995) with a water channel used to investigate RT instability-driven turbulent mixing. Novel experimental techniques were developed, combining passive scalar and reacting flow measurements at various equivalence ratios to obtain resolution-independent measurements of mean and fluctuating density statistics. These results were used to calculate various parameters quantifying the degree of molecular mixing. This paper is organized as follows. First, an overview of the water channel facility, indicator chemistry and optical diagnostics are presented in § 2. Measurements of the coloured chemical product formation are then presented in § 3, and the results are compared with the $Sc \sim 10^3$ shear-driven mixing results of Breidenthal (1979, 1981) to show that the diagnostic is operating correctly. The chemical product measurements are used to obtain the first resolution-independent measurements for the $Sc \sim 10^3$ case of several commonly used parameters that quantify the degree of molecular mixing in § 4. A relationship between the chemical product formed and the density variance is developed; comparisons of the molecular mixing parameter θ are given for the $Sc = 0.7$ (Kraft *et al.* 2009), $Pr \equiv Sc = 7$ (Mueschke *et al.* 2006) and $Sc \sim 10^3$ cases; and the results are discussed. The implications of these measurements for the development and assessment of turbulent transport and mixing models are discussed in § 5, and the paper closes with conclusions in § 6.

2. Experimental facility

Experiments were performed using an open-loop water channel facility (Snider & Andrews 1994; Wilson & Andrews 2002; Ramaprabhu & Andrews 2004; Mueschke

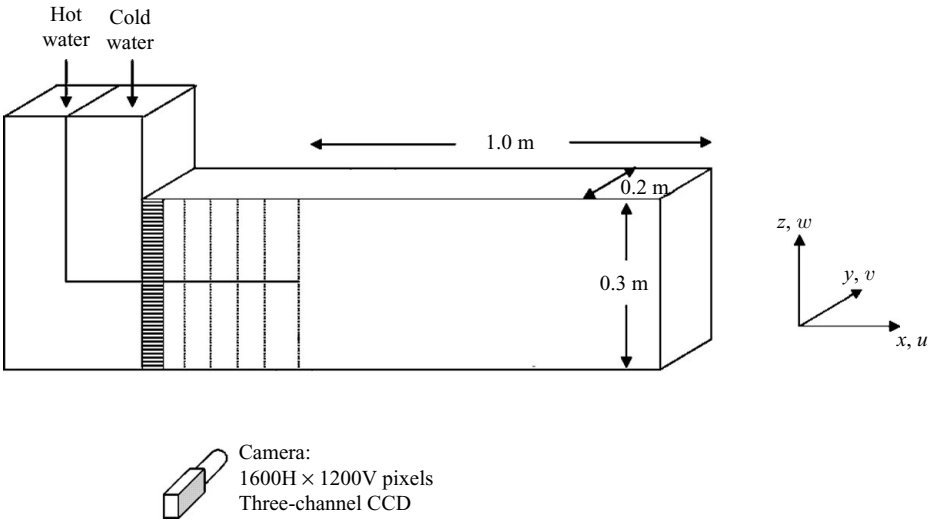

FIGURE 1. Schematic of the water channel and the associated coordinate system.

et al. 2006) supplied by two 500 gallon water tanks (see figure 1). Two streams of water were pumped into the channel and separated by a thin splitter plate. Care was taken to ensure that the flow stream velocities were matched by verifying that tracked dye markers did not move relative to one another as they were advected downstream. A series of flow straighteners and wire meshes mitigated free-stream turbulence and boundary layers (Browand & Weidman 1976; Koop 1976; Stillinger *et al.* 1983) to the extent that the free-stream turbulence was negligible (Snider & Andrews 1994). An unstable stratification of a heavier fluid over a lighter fluid developed downstream of the splitter plate, which transitioned to a turbulent RT mixing layer as the heavier fluid fell and the lighter fluid rose. Snider & Andrews (1994) studied the influence of the distance between the front and back walls of the channel on the development of the RT mixing layer and found that the width should be at least half of the depth to avoid late-time interference with the development of large structures. Moreover, they indicated that the RT mixing layer width is not affected by the top and bottom walls until the channel is at least 80 % filled. Both criteria were fulfilled in the present experiments. The layer was advected downstream by a mean velocity $U_m \approx 5\,\mathrm{cm\,s^{-1}}$ that gives parabolic flow for the developed RT mixing layer (Snider & Andrews 1994), and the time evolution was related to downstream distance by Taylor's hypothesis $t = x/U_m$ (Pope 2000). Using the same facility and flow conditions (Atwood number, advection velocity and no shear) Ramaprabhu & Andrews (2004) measured negligible skewness of the axial velocity root mean square (r.m.s.) fluctuations, indicating a 'frozen' condition in the axial direction and thus justifying Taylor's hypothesis. Indeed, another criterion (Pope 2000) for the Taylor hypothesis is $u'/\overline{U} \ll 1$; i.e. the axial velocity fluctuation is much less than the advective velocity. A small spread angle was designed in the experiment to ensure that the flow was parabolic, so that $w'/\overline{U} \ll 1$ (Snider & Andrews 1994). Ramaprabhu & Andrews (2004) reported $u'/w' \approx 0.5$, and thus the $u'/\overline{U}$ criterion was also satisfied in the present experiment. Time was normalized by

$$\tau = t\sqrt{\frac{A\,g}{H}}, \tag{2.1}$$

	Diffusivity ($cm^2\ s^{-1}$)	Sc
Na^+	1.334×10^{-5}	750
Cl^-	2.032×10^{-5}	492
NaCl	1.611×10^{-5}	620
H^+	9.311×10^{-5}	107
OH^-	5.273×10^{-5}	190
Phenolphthalein	8.3×10^{-6}	1200

TABLE 1. Species diffusivities in water at 20°C (Desai & Vadgama 1991; Lide 2006).

where $H = 32\,\text{cm}$ is the vertical height of the channel. The water channel provides a unique facility for measuring turbulence statistics, as the RT mixing layer is statistically stationary, and long sampling times are available.

In the experiments presented here, salt (NaCl) was added to the top stream of the channel to create a density difference with an Atwood number 7.5×10^{-4}. In this case, the concentration of salt served as a marker for the density field. The resulting species diffusivity of the Na^+ and Cl^- ions (see table 1) gave a Schmidt number $Sc = 620$ (Lide 2006). Direct measurements of the salt concentration field were not feasible due to the large magnitudes of the scalar gradients (Mueschke & Andrews 2005*a*, *b*). Instead, a diffusion-limited chemical reaction between the two streams was monitored to measure the degree of molecular mixing. The pH of each stream was altered by adding either hydrochloric acid (HCl) or sodium hydroxide (NaOH) to each stream. As the two fluids molecularly mixed, a neutralization reaction occurred, and the local pH of the mixture reached a new equilibrium. The reaction was monitored by the addition of a pH-sensitive chemical indicator (phenolphthalein) to the acidic stream. As the local pH of the mixture changed, the transparent phenolphthalein changed colour to a translucent shade of pink. The concentration of the coloured form of the indicator was measured using backlit optical techniques. This section presents an overview of the prerequisite chemistry, optical measurement techniques and estimated measurement uncertainty bounds.

2.1. *Reaction chemistry*

In the current experiments, fluid 1 is the heavier fluid with $\text{pH}_1 > 7$ (alkali), and fluid 2 is the lighter fluid with $\text{pH}_2 \leqslant 7$ (either acidic or neutral), where the subscript denotes either the top (heavy) or bottom (light) stream. In aqueous solutions, the concentration of hydrogen and hydroxide ions remains balanced according to the reversible reaction

$$H_2O \Leftrightarrow H^+ + OH^- \tag{2.2}$$

with associated equilibrium constant

$$K_w = [H^+]\,[OH^-] = 1 \times 10^{-14}, \tag{2.3}$$

where square brackets denote molar concentration, i.e. moles per liter (Harris 2003). As fluid from each stream molecularly mixes, the local concentrations of H^+ and OH^- adjust to a new equilibrium value satisfying (2.3). The pH of the resulting mixture is $\text{pH}_{mix} = -\log_{10}\,[H^+]_{mix}$. Further details on the neutralization reaction are given in the Appendix.

In this work, the pH is controlled by the addition of HCl or NaOH to either stream. Given the stoichiometric quantities of HCl and NaOH (i.e. both reactants are completely consumed in the reaction) the resulting mixture reacts according to the

exothermic reaction $HCl\,(aq) + NaOH\,(aq) \longrightarrow H_2O\,(l) + NaCl\,(aq)$ with heat release $\Delta h_f^0 = -59.8$ kJ mol^{-1}. Given a specific heat capacity of water $C_p = 4.179$ J g^{-1} K^{-1}), the local temperature increase in the fluid is $\Delta T \approx 0.02^{\circ}$C for the case of $pH_1 = 11.5$ and $pH_2 = 2.5$. Accordingly, the local decrease in density due to thermal expansion is negligible, and thus, the neutralization reaction has a negligible effect on the Atwood number or on the buoyancy effects driving the mixing.

To monitor the neutralization reaction, a small quantity of phenolphthalein ($C_{20}H_{14}O_4$) indicator was dissolved in the bottom (acidic) stream; the notation 'In' denotes the indicator. Typical concentrations of $[In]_2 = 6 \times 10^{-6}$ mol L^{-1} were used, where the subscript indicates that the indicator was added to the bottom stream. While the chemistry of the neutralization reaction is straightforward, the chemistry of the pH-sensitive indicator is complex. Phenolphthalein is a weak acid and will dissociate depending upon the local pH (Bishop 1972). Schematically, the indicator follows the reversible reaction

$$\text{Transparent indicator} + 2OH^- \Leftrightarrow \text{Coloured indicator}. \tag{2.4}$$

Phenolphthalein has multiple ionization states and, thus, several different chemical forms (denoted by Roman numeral subscripts):

$$In_{I} \Leftrightarrow In_{III} + H^+, \tag{2.5}$$

$$In_{III} \Leftrightarrow In_{IV} + H^+, \tag{2.6}$$

$$In_{III} \Leftrightarrow In_{VII} + 2H^+. \tag{2.7}$$

All forms of the indicator in (2.5)–(2.7) are transparent with the exception of the pink quinone phenolate form (In_{IV}). The equilibrium constants for the first two reactions are (Kolthoff 1937)

$$K_1 = \frac{[In_{III}][H^+]}{[In_{I}]} = 1.15 \times 10^{-9}, \tag{2.8}$$

$$K_2 = \frac{[In_{IV}][H^+]}{[In_{III}]} = 2.8 \times 10^{-10}. \tag{2.9}$$

As the pH of a mixture rises above 8, the equilibria of (2.5) and (2.6) move to the right according to Le Chatelier's principle, and the coloured form of the indicator is produced. However, when pH > 11.3, the equilibrium of the reaction in (2.7) also moves to the right, and consequently, less In_{III} is available for the reaction in (2.6), and less coloured indicator In_{IV} is formed. Zhang *et al.* (1995) reported a measurement of the equilibrium constant

$$K_3 = \frac{[In_{VII}][H^+]^2}{[In_{III}]} \approx 2.75 \times 10^{-23} \tag{2.10}$$

for this reaction. An expression for the fraction of indicator in its coloured form can be obtained by substituting the equilibrium constants (2.8)–(2.10) into the mass balance equation

$$[In] = [In_{I}] + [In_{III}] + [In_{IV}] + [In_{VII}]. \tag{2.11}$$

Solving for $[In_{IV}]/[In]$ gives a relative measure of In_{IV} concentration as a function of H^+ concentration (Harris 2003). The fraction of dissociation of In_{IV},

$$\alpha_{In_{IV}} = \frac{[In_{IV}]}{[In]} = \frac{K_1 K_2}{K_1 K_2 + K_1 [H^+] + [H^+]^2 + K_1 K_3 [H^+]^{-1}}, \tag{2.12}$$

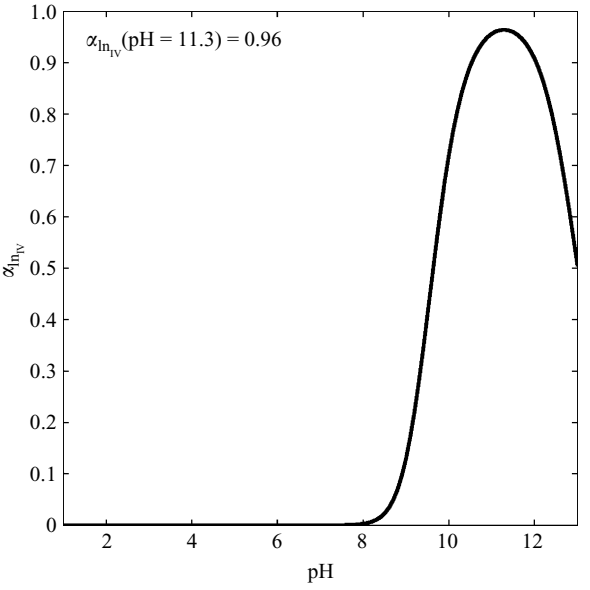

FIGURE 2. Fraction of dissociation for the coloured form of the chemical indicator $\mathrm{In_{IV}}$.

is defined such that $\alpha_{\mathrm{In_{IV}}} = 0$ when none of the indicator is in its coloured form, and $\alpha_{\mathrm{In_{IV}}} = 1$ when all of the indicator is in its coloured form. Figure 2 shows the fraction of dissociation $\alpha_{\mathrm{In_{IV}}}$ as a function of pH.

2.2. *Optical imaging system and calibration*

All constituents of the mixing layer and forms of the chemical indicator are transparent except for the final product $\mathrm{In_{IV}}$, which absorbs green light ($\lambda_{peak} = 552\,\mathrm{nm}$) and is therefore pink (Green 1990). The attenuation of a light ray passing through the mixing layer is related to the concentration of coloured indicator $[\mathrm{In_{IV}}]$ through the Beer–Lambert law (Hecht 2002)

$$\sigma = \varepsilon \int_0^L [\mathrm{In_{IV}}]\,\mathrm{d}y, \tag{2.13}$$

where σ is the absorption of light, ε is a molar absorptivity constant for phenolphthalein, and L is the total path length of the light ray through the absorbing medium. The absorption of light is related to the ratio of measured light intensity I to the backlighting intensity I_0 by

$$\sigma = -\ln\left(\frac{I}{I_0}\right) = \varepsilon\, L\, \overline{\overline{[\mathrm{In_{IV}}]}}, \tag{2.14}$$

where $\overline{\overline{[\mathrm{In_{IV}}]}}$ is the spanwise average concentration of coloured indicator. In this work, the double overbar denotes a spatial average across the span of the channel along a light ray. Thus, given a calibrated value of the molar absorptivity, ε, $\overline{\overline{[\mathrm{In_{IV}}]}}$ is linearly related to a light absorption measurement. Coloured indicator concentration measurements normalized by the free-stream indicator concentration $C = \overline{[\mathrm{In_{IV}}]}/[\mathrm{In}]_2$ are presented in § 3.2, where the single overbar denotes an average of $\overline{[\mathrm{In_{IV}}]}$ over a series of individual images.

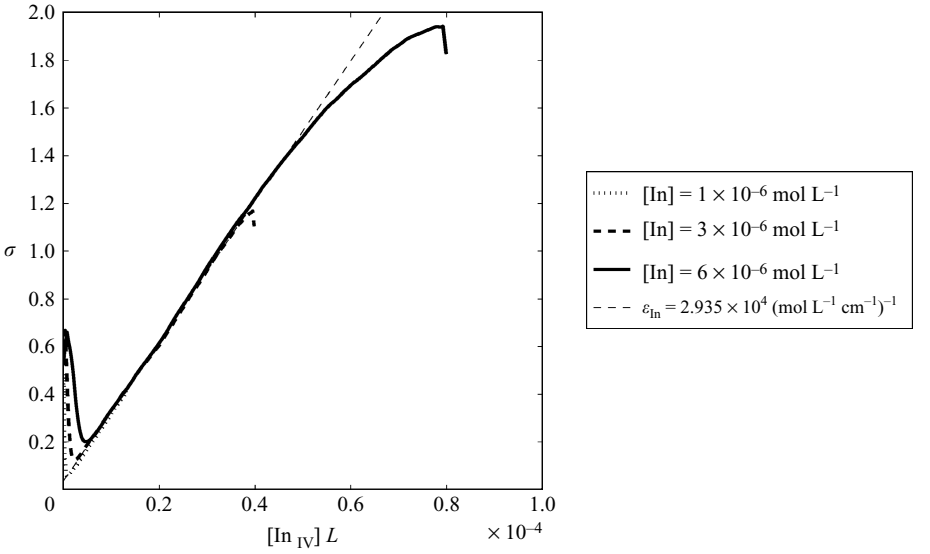

FIGURE 3. Calibration of molar absorptivity coefficient $\varepsilon_{\mathrm{In}}$ for phenolphthalein. A fiducial for $\varepsilon_{\mathrm{In}} = 2.935 \times 10^4$ (mol L^{-1} $\mathrm{cm}^{-1})^{-1}$ is shown (dashed line).

In the present work, the molar absorptivity coefficient of phenolphthalein was measured by filling a Plexiglas wedge with a known concentration of indicator at a specified pH. The variation in light absorption across the wedge provided a measure of the light absorption versus depth of the wedge. The molar absorptivity coefficient was measured by calculating the slope of the absorption curve shown in figure 3. The rise in absorptivity at the low end of the concentration range is due to the convergence of the Plexiglas width and internal reflections, giving the appearance of a thicker layer – an effect noticed by Snider & Andrews (1994) when calibrating dye absorption. Aside from previous work that indicates a rise in absorptivity at the thin end of the wedge, we also note that the rise in absorptivity of the lowest concentration indicator (10^{-6} mol L^{-1}) narrows at the thin end of the wedge, whereas if a nonlinearity were present it would widen (i.e. it would take more indicator to reach the linear growth). The calibration experiment was repeated using three different indicator concentrations: each produced similar slopes such that $\varepsilon_{\mathrm{In}} = 2.935 \times 10^4 \pm 0.67\,\%$ (mol L^{-1} $\mathrm{cm}^{-1})^{-1}$, which agreed well with the value $\varepsilon_{\mathrm{In}} = 2.934 \times 10^4$ (mol L^{-1} $\mathrm{cm}^{-1})^{-1}$ measured by Zhang *et al.* (1995). It was found that the system response became nonlinear for absorptions $\sigma > 1.5$, so the phenolphthalein concentration in the acidic stream was limited to exclude absorptions $\sigma > 1.2$.

To measure the concentration of the coloured form of phenolphthalein in the channel, the experiment was backlit by multiple fluorescent lights. Prismatic panels and sheets of translucent velum were placed between the light source and the mixing section of the channel to create a uniform backlighting source. Attenuation of the background lighting by the coloured phenolphthalein indicator was measured using an 8 bit, three-channel colour CCD array incorporated in a 4 megapixel Canon Powershot® A80 camera operated in high-speed continuous capture mode with settings of ISO 100, shutter speed 1/60 s and aperture $f/7.1$. The camera was placed 5 m from the tank and zoomed on the water channel to minimize parallax effects, giving a typical image of the flow channel with depth (30 cm) and length (100 cm) covered by 300 × 1000 pixels and hence a spatial resolution of 1 mm. A green optical

filter was used to minimize the transmission of wavelengths above and below the peak absorption wavelength of phenolphthalein to the CCD array. Approximately 200 photographs were used to measure the average light absorption by the indicator. The light absorption from all the images were averaged to calculate the averaged concentration $\overline{[\mathrm{In}_{\mathrm{IV}}]}$ through the Beer–Lambert law (2.14), where the single overbar denotes time and spatial averaging in the spanwise direction.

The optical imaging techniques employed in this work are similar to those of Breidenthal (1979, 1981) and Zhang *et al.* (1995) and quantify the amount of chemical product formed, given a diffusion-limited chemical reaction. The amount of backlighting absorbed by the chemical indicator at any spatial location is independent of the camera resolution used to record the digital images. Accordingly, the analysis presented in § 3 and § 4 is free of artificial filtering of the scalar fluctuations by probe resolution limitations.

2.3 *Uncertainty analysis*

The density difference between the two fluids was created by adding salt to the top stream. The density of each fluid was obtained by measuring the mass of a 50 mL sample in a high-accuracy flask on an electronic balance. Multiple samples were measured ($N \approx 8$–10), and the density of each fluid stream $\rho_i = m_i/V$ (where $i = 1, 2$ denotes the top and bottom streams) was determined. The 95 % confidence interval bounds were obtained from

$$w_{m_i} = \pm 1.96\sqrt{\frac{s_{m_i}^2}{N}}, \tag{2.15}$$

where $s_{m_i}^2$ is the variance of the mass measurements and N is the number of samples (Benedict & Gould 1996). The resulting uncertainty in the density of each fluid is

$$w_{\rho_i} = \pm\sqrt{\left(\frac{\partial \rho_i}{\partial m_i} w_{m_i}\right)^2 + \left(\frac{\partial \rho_i}{\partial V} w_V\right)^2}, \tag{2.16}$$

where $w_V = \pm 0.05$ mL is the uncertainty in the volume measurement. Similarly, the uncertainty in the Atwood number for a given experiment is

$$w_A = \pm\sqrt{\left(\frac{\partial A}{\partial \rho_1} w_{\rho_1}\right)^2 + \left(\frac{\partial A}{\partial \rho_2} w_{\rho_2}\right)^2} = \pm 1\ \%. \tag{2.17}$$

The velocity of each stream was measured by injecting dye into the top and bottom streams and recording the time required for the dye to travel a measured distance. Using similar uncertainty propagation estimates as in (2.16) and (2.17), the mean advection velocity of the two streams was known to within ± 2 %. The uncertainty in the mean advection velocity was the greatest contributor to the uncertainty of the dimensionless time τ (see (2.1)), which was also known to within ± 2 %.

Uncertainties in the mean coloured indicator concentration measurements were due to several sources, including the uncertainty in the free-stream indicator concentration $w_{[\mathrm{In}]_2}$, the molar absorptivity coefficient w_ε, the light absorption measurement w_σ and the channel width w_{L_y}. Furthermore, uncertainty in the phenolphthalein concentration in the bottom stream was determined by uncertainties in the volume of phenolphthalein added (± 5 mL) and the volume of water in the bottom stream tank (1890 ± 2 % L). Together this gives a relative uncertainty in the chemical indicator concentration in the bottom stream of ± 1.4 %. The molar absorptivity coefficient from the calibration experiments in § 2.3 was determined to have an uncertainty of ± 0.67 %. Finally, uncertainty in the light absorption measurements were due to variations in

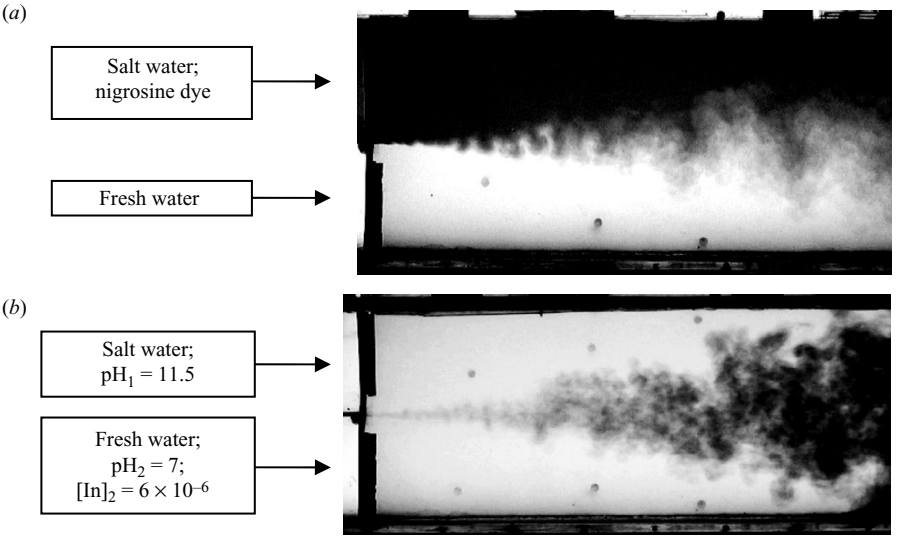

FIGURE 4. Photographs (contrast enhanced for visualization) of the buoyancy-generated mixing layer in a typical water channel experiment. (*a*) Nigrosine dye was added to the top stream. (*b*) Phenolphthalein was added to the bottom stream, which changes to its pink form as the two streams molecularly mix (here, "pink" is shown as dark regions within the mixing layer).

the background lighting intensity and statistical uncertainty in the estimation of the mean light intensity measured from an ensemble average of ~200 images determined previously by Ramaprabhu & Andrews (2004) to give well-converged statistics. The r.m.s. amplitude of the background lighting fluctuations was 0.8 intensity units on a scale of 0–255 from the 8 bit CCD. Accordingly, the intensity of the background lighting was steady to within $\pm 0.5\,\%$. Combining all of these uncertainties gives an uncertainty of the measured chemical concentration C of

$$w_C = \pm\sqrt{\left(\frac{\partial C}{\partial \sigma} w_\sigma\right)^2 + \left(\frac{\partial C}{\partial \varepsilon} w_\varepsilon\right)^2 + \left(\frac{\partial C}{\partial L_y} w_{L_y}\right)^2 + \left(\frac{\partial C}{\partial [\mathrm{In}]_2} w_{[\mathrm{In}]_2}\right)^2} = \pm 3\,\%. \tag{2.18}$$

3. Passive scalar and chemical indicator measurements

3.1. *Measurement of mixing layer growth*

As an initial check of the experimental facility and diagnostics, the RT mixing layer width was measured for the salt/fresh water configuration. Nigrosine dye (5 g) was added to the tank supplying the top stream, and the absorption of light was measured using the techniques discussed in § 2.2. A sample image from an experiment using the inert dye is shown in figure 4. The dye absorptivity coefficient was measured using the same Plexiglas wedge and light absorption techniques discussed in § 2.2. Experiments using the dye were then performed, and the absorption of the backlighting was related to the mean dye concentration. The mean dye concentration was normalized by the free-stream dye concentration and related to the mean heavy fluid (top stream) volume fraction by

$$\bar{f}_1 = \frac{\bar{\rho} - \rho_2}{\rho_1 - \rho_2} = \frac{\overline{[Dye]}}{[Dye]_1}, \tag{3.1}$$

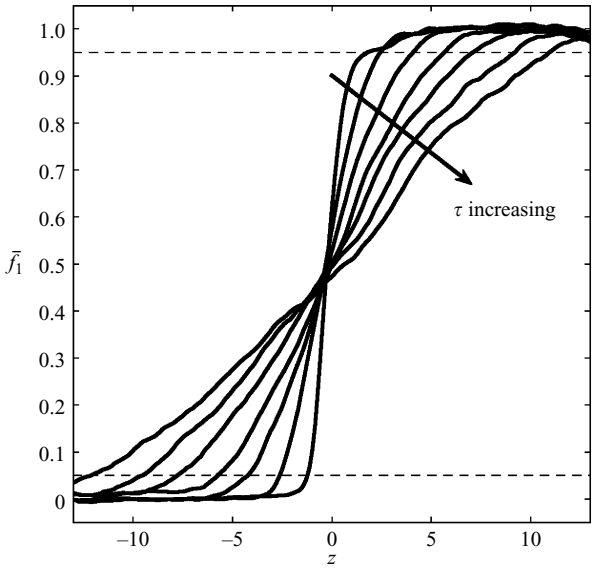

FIGURE 5. Mean volume fraction profiles across the mixing layer at dimensionless times $\tau = 0.25$, 0.50, 0.75, 1.00, 1.25 and 1.50. Fiducials indicating the boundaries of the mixing layer are shown at $\bar{f}_1 = 0.05$ and $\bar{f}_1 = 0.95$.

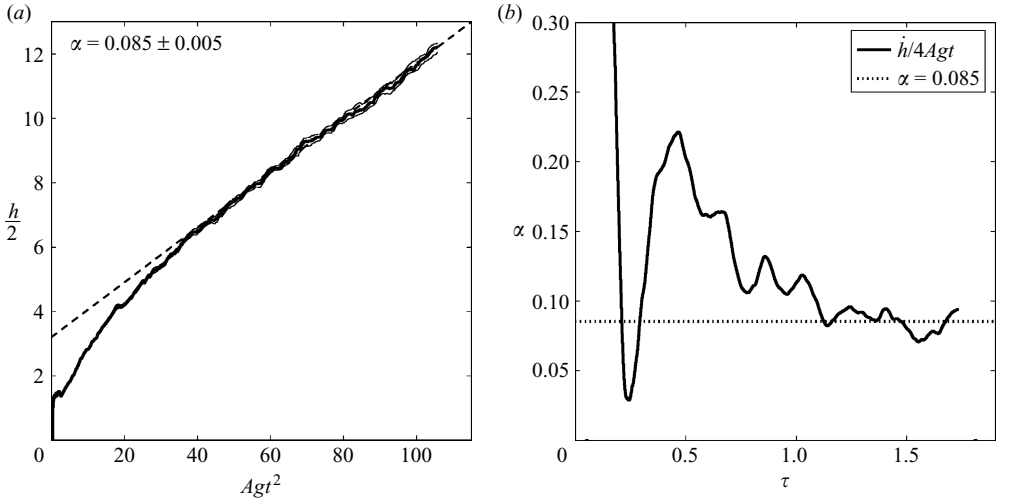

FIGURE 6. Measurement of the mixing layer growth parameter α for the $Sc \sim 10^3$ case. (*a*) The half-width of the mixing layer is plotted against Agt^2 with 95 % confidence interval bounds. (*b*) An alternative measure of α is obtained by dividing $\dot{h}$ by $4Agt$. In both (*a*) and (*b*), a fiducial is shown for $\alpha = 0.085$ (dashed line).

where $\bar{f}_1$ is a dimensionless measure of the mean density field. Profiles of $\bar{f}_1$ at several downstream locations are shown in figure 5. As expected for small Atwood number RT mixing (Youngs 1984; Snider & Andrews 1994), the growth of the RT mixing layer is symmetric about $\bar{f}_1 = 0.5$ with approximately linear profiles. The RT mixing layer width was determined by identifying the 5 %–95 % thresholds from the $\bar{f}_1$ profiles. The growth parameter $\alpha = 0.085 \pm 0.005$ was obtained by measuring the slope of the half-width of the RT mixing layer plotted against Agt^2, as shown in figure 6.

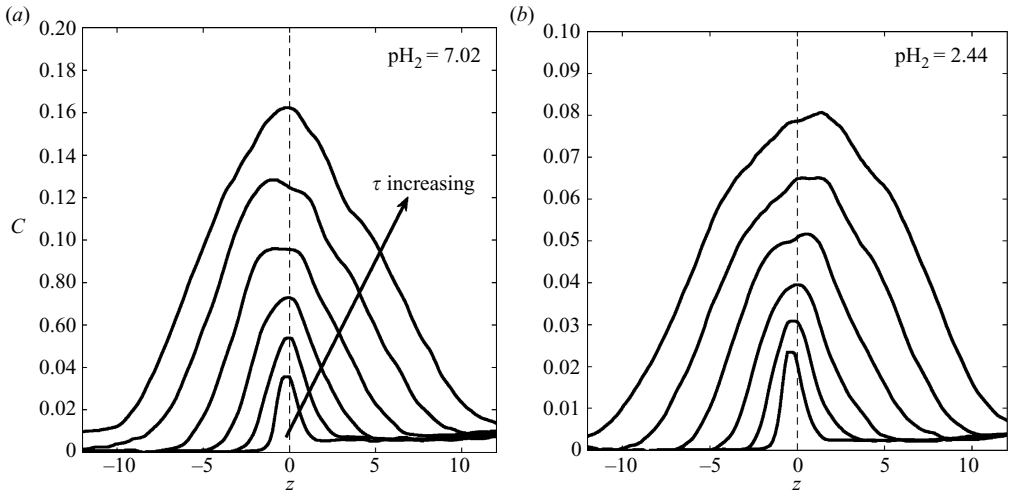

FIGURE 7. Normalized coloured indicator concentration profiles across the mixing layer at dimensionless times $\tau = 0.25$, 0.50, 0.75, 1.00, 1.25 and 1.50 for the (*a*) $pH_2 = 7.02$ and (*b*) $pH_2 = 2.44$ cases, with $pH_1 \approx 11.5$ for both experiments.

Ristorcelli & Clark (2004) showed that a measurement of α directly from (1.1) is not independent of additional terms that scale as t^1 and t^0. The dependence on such additional terms can be minimized by measuring α from the time derivative $\dot{h} = 4\alpha Agt$ instead. Thus, the 'instantaneous' value of $\alpha = \dot{h}^2/(8Agh)$ from Ristorcelli & Clark (2004) is also shown in figure 6 as a confirmation, where a self-similar asymptotic value of $\alpha = 0.086 \pm 0.01$ is measured for $\tau \geqslant 1.1$. While this measure has a larger degree of statistical uncertainty due to the time derivative of h, both values of α are consistent. The growth parameter for the salt/fresh water case is slightly larger than that for the hot/cold water case, where $\alpha = 0.07 \pm 0.011$ (Snider & Andrews 1994). Thus, the increase in α for the salt/fresh water case suggests that the Schmidt number may have only a minor influence on the late-time RT mixing layer width.

3.2. *Measurements of chemical product formation*

Using the backlit optical techniques described in § 2.2, the average concentration of the coloured chemical indicator was measured in a turbulent RT mixing layer. Figure 4 shows an image of the layer, where the pink chemical indicator represents regions of mixed fluid (the pink region is shown as the dark region in Fig. 4(b)). Figure 7 shows the profiles of $C = \overline{[\mathrm{In}_{\mathrm{IV}}]}/[\mathrm{In}]_2$ (the concentration of coloured indicator normalized by the free-stream concentration) for $pH_2 = 7.02$ and $pH_2 = 2.44$. The resulting profiles are approximately parabolic, and, as expected, less chemical product is produced in the latter case. Figure 7(*b*) shows a slight bias in the absorption measurements due to inherent absorption by the weak salt solution and was determined to be less than the statistical uncertainty of the measurement. By decreasing the pH of the bottom stream, the concentration of H^+ ions is increased, so that the quantity of OH^- ions required to mix with the bottom stream to achieve a colour change in the indicator is increased. Therefore, given the same degree of molecular mixing between the two streams, less coloured indicator is produced when the pH of the bottom stream is lowered. In the $pH_2 = 7.02$ and $pH_2 = 2.44$ cases, the measured concentration of the coloured indicator increases as the RT mixing layer grows spatially downstream: this is expected, as the intensity of turbulence increases and as the internal structure becomes more complex with increasing Reynolds numbers.

Turbulent fluctuations continuously stretch the interface between pockets of fresh and salt water, which increases the reaction surface area and brings fresh reactants into contact.

Previous researchers found that the quantity of indicator produced is a function of the equivalence ratio ϕ and is a measure of balance or excess of reactants. Typically, the equivalence ratio for shear and jet flows is defined for the reaction involving the chemical indicator (see (2.4)) such that

$$\phi_{\mathrm{In}} = \frac{[\mathrm{In}]/[\mathrm{OH}^-]}{([\mathrm{In}]/[\mathrm{OH}^-])_{st}}, \tag{3.2}$$

where $([\mathrm{In}]/[\mathrm{OH}^-])_{st} = 1/2$ is the stoichiometric ratio of reactants in (2.4). In the limit $\phi_{\mathrm{In}} \to 0$, the quantity of coloured chemical indicator C produced attains an asymptotic value and is a function only of the degree of molecular mixing between the two fluids (Shea 1977; Breidenthal 1979, 1981; Mungal & Dimotakis 1984; Zhang *et al.* 1995).

The equivalence ratio for the indicator reaction neglects the neutralization reaction in (2.2) that occurs as fluid from each stream mixes. Accordingly, ϕ_{In} does not account for the reduced quantity of indicator formed in the $\mathrm{pH}_2 = 2.44$ experiment. To account for this effect, it is more appropriate to examine the equivalence ratio of the neutralization reaction in (2.2), where

$$\phi_n = \frac{[\mathrm{H}^+]/[\mathrm{OH}^-]}{([\mathrm{H}^+]/[\mathrm{OH}^-])_{st}} \tag{3.3}$$

and $([\mathrm{OH}^-]/[\mathrm{H}^+])_{st} = 1$ is the stoichiometric ratio of hydroxide and hydrogen ions. The neutralization equivalence ratio ϕ_n controls the volume fractions of fluid 1 and fluid 2 that must mix to achieve the pH increase required for the indicator to change colour. For $\phi_n \to 0$, a large excess of OH^- ions exists in the top stream, and only a small fraction of fluid 1 must mix with fluid 2 to achieve a significant pH increase and resulting indicator colour change. Conversely, for $\phi_n \to \infty$, a large excess of H^+ ions exists, and an infinite amount of fluid 1 is required to mix with fluid 2 to achieve the required pH increase. As a result, no indicator will be converted to its coloured form. For the pH combination $\mathrm{pH}_1 = 11.5$ and $\mathrm{pH}_2 = 7$, $\phi_n = 3.2 \times 10^{-5} \ll 1$, and only a small fraction of fluid 1 is required to mix with fluid 2 to achieve a colour change. Accordingly, a measure of C for $\phi_{\mathrm{In}} = 1.8 \times 10^{-3}$ and $\phi_n = 3.2 \times 10^{-5}$ ($\mathrm{pH}_1 = 11.5$, $\mathrm{pH}_2 = 7$, $[\mathrm{In}]_2 = 6 \times 10^{-6}$) should be insensitive to the exact equivalence ratio and representative of the degree of molecular mixing.

3.3. *Species diffusivity considerations*

In previous work examining high-Schmidt-number liquid-phase mixing (Breidenthal 1979, 1981; Koochesfahani & Dimotakis 1986; Linden *et al.* 1994; Zhang *et al.* 1995), acid–base neutralization reactions coupled with pH-sensitive chemical indicators quantified the degree of molecular mixing. While it is customary to estimate $Sc \sim 10^3$ in liquid-phase mixing, each specific molecule or ion within the mixture diffuses at a different rate. Table 1 lists the species diffusivities and their respective Schmidt numbers for the current experiments. It is important to note that the neutralization reaction front will precede the indicator reaction front because of the relatively high diffusivities of H^+ and OH^-. Accordingly, the total quantity of coloured indicator is not limited by the diffusivities of the H^+ and OH^- ions. Larger ions, such as those of sodium and chloride, have lower mobilities, resulting in an effective Schmidt number $Sc_{\mathrm{NaCl}} = \nu/D_{\mathrm{NaCl}} = 620$ (Lide 2006). The diffusivity of phenolphthalein was measured

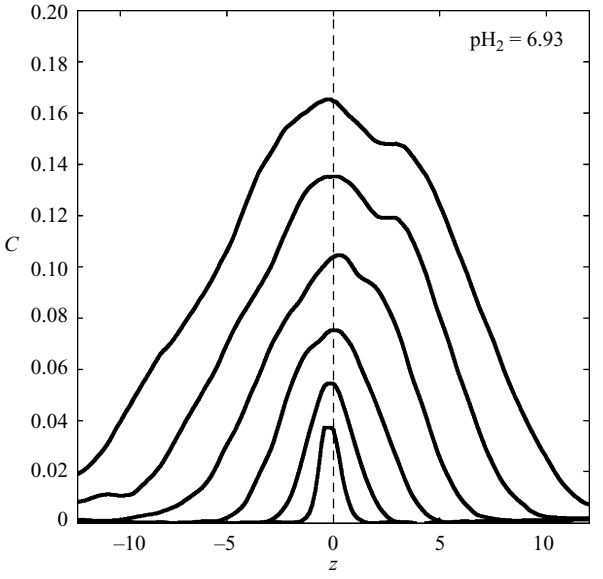

FIGURE 8. Normalized coloured indicator concentration profiles across the mixing layer at $\tau = 0.25$, 0.50, 0.75, 1.00, 1.25 and 1.50 for the hot/cold water case.

by Desai & Vadgama (1991), giving an indicator Schmidt number $Sc_{\mathrm{In}} = \nu/D_{\mathrm{In}} = 1200$. Due to the difference in Sc_{NaCl} and Sc_{In}, the nominal Schmidt number of the experiments reported here is considered to be $Sc \sim 10^3$.

An experiment was performed using a temperature increase in the bottom fluid stream ($\Delta T \approx 5^{\circ}\mathrm{C}$) to create a density difference in order to demonstrate that the diffusivity of the chemical indicator determines the nominal Schmidt number. For this reference experiment, the pH of each stream was set to $\mathrm{pH}_1 \approx 11.5$ and $\mathrm{pH}_2 \approx 7$ to match ϕ_{In} and ϕ_n of the baseline salt/fresh water experiments. No salt was added to the top stream, and thus the temperature of the water becomes a marker for the density field through an equation of state (Kukulka 1981). In this arrangement, the nominal Schmidt number of the scalar marking the density field is equivalent to the Prandtl number $Pr = 7 \equiv Sc$; however, the Schmidt number for the chemical indicator remains unchanged at $Sc_{\mathrm{In}} = 1200$. Measurements of the coloured indicator concentration for this hot/cold water case are shown in figure 8. These profiles indicate that similar amounts of coloured chemical product are produced, despite the increased scalar diffusivity and presumably increased amount of mixed fluid within the layer. This experiment demonstrates that the diffusivity of the indicator limits its use to flows in which the diffusivity of the scalar marking the density field is similar to the diffusivity of the indicator. In the present experiments, the diffusivity of Na^+ and Cl^- ions in water gives an effective Schmidt number $Sc_{\mathrm{NaCl}} = 620$ (Lide 2006), which is a factor of two smaller than $Sc_{\mathrm{In}} = 1200$. It will be shown in §4.2 that a factor of 10 difference in Schmidt numbers results in only a small change in the molecular mixing parameter θ, and thus, a factor of two difference in the Schmidt numbers of salt and phenolphthalein is considered negligible.

3.4. *Product thickness integrals*

An integral measure quantifying the amount of chemical product formed (and representing the fraction of the mixing layer occupied by the coloured indicator)

is the equivalent product thickness

$$\frac{P}{h} = \frac{1}{h}\int_{-h/2}^{h/2} \frac{\overline{[\mathrm{In}_{\mathrm{IV}}]}}{[\mathrm{In}]_2}\,\mathrm{d}z, \tag{3.4}$$

which is analogous to P/δ for shear flows (Konrad 1977; Breidenthal 1979, 1981). For all experiments that used salt to create a density difference, a correction to (3.4) was applied to account for the absorption of light by the salt water from the measurement of P:

$$\frac{P}{h} = \frac{1}{h}\left[\int_{-h/2}^{h/2} \frac{\overline{[\mathrm{In}_{\mathrm{IV}}]}}{[\mathrm{In}]_2}\,\mathrm{d}z - \frac{h}{2}\xi\right], \tag{3.5}$$

where $\xi \approx 0.0075$ is the value of C measured outside the RT mixing layer in the salt water stream.

To validate the diagnostic techniques described in § 2.2, the water channel was used to create a reacting, turbulent shear layer similar to the flow created by Breidenthal (1979, 1981). The pH of each stream was set to $\mathrm{pH}_1 = 11.73$ and $\mathrm{pH}_2 = 7.04$ to match Breidenthal's (1979, 1981) conditions. The indicator concentration was set to $[\mathrm{In}]_2 = 5 \times 10^{-6}$ mol L^{-1}, whereas Breidenthal (1979, 1981) used $[\mathrm{In}]_2 = 1 \times 10^{-5}\,\mathrm{mol\,L^{-1}}$. The indicator concentration in the current experiments was lowered to keep the diagnostics in the linear range of the calibration. Salt was also added to the bottom stream as necessary to balance the increased density of the top stream due to the addition of NaOH, so that $\rho_1 = \rho_2$. The velocities of the top and bottom streams in the channel were adjusted to $U_1 = 5.8\,\mathrm{cm\,s^{-1}}$ and $U_2 = 3.5\,\mathrm{cm\,s^{-1}}$, respectively, giving a velocity ratio $r = U_2/U_1 = 0.61$. While Breidenthal (1979, 1981) reported results for $r =$ 0.38–0.80, the absolute velocities of each stream were much larger than those in the current water channel. In Breidenthal's (1979, 1981) work, the high-speed stream was $U_1 = 300\,\mathrm{cm\,s^{-1}}$, with a resulting low-speed stream velocity $U_2 = rU_1$. In addition, Breidenthal's (1979, 1981) facility used a series of flow straighteners and meshes and included a large cross-sectional area contraction to minimize boundary layers on the splitter plate and adjustable side walls to account for streamwise pressure gradients. The water channel experiments also use a series of flow straighteners and screen meshes to control boundary layers on the splitter plate, but no contraction was implemented. Due to differences in facility designs and flow velocities, the initial conditions for each experiment are not identical. Breidenthal (1979, 1981) reported that P/δ is a non-unique function of Reynolds number for $Re_\delta < 8000$. This was attributed to the observation that early-time, two-dimensional vorticity dynamics of the mixing layer were controlled by the initial vorticity in the high-speed fluid boundary layer. Remnants of initial conditions affected the value of P/δ until the mixing layer had completely transitioned to a fully developed, three-dimensional state. Thus, slightly different initial conditions resulted in different measures of P/δ before the asymptotic value $P/\delta \approx 0.365$ for $Re_\delta > 8000$ was reached.

Figure 9 shows a comparison of P/δ for $r = 0.62$ and $r = 0.76$ from Breidenthal (1979) and a corresponding shear layer experiment conducted in the current water channel as a function of shear layer Reynolds number $Re_\delta = \Delta U/\delta\nu$, where $\delta = \Delta U/(\partial u/\partial z)_{max}$ is the vorticity thickness of the shear layer. In the absence of velocity measurements to obtain δ directly, the width of the shear layer was determined visually from the measured indicator concentration profiles. The visual width of the mixing layer δ_{vis} is related to the vorticity thickness δ such that $\delta_{vis}/\delta = 2.1$ (Brown & Roshko 1974; Koochesfahani & Dimotakis 1986). The water channel Reynolds numbers were limited to $Re_\delta < 2000$. Thus, the asymptotic value $P/\delta \to 0.365$ for

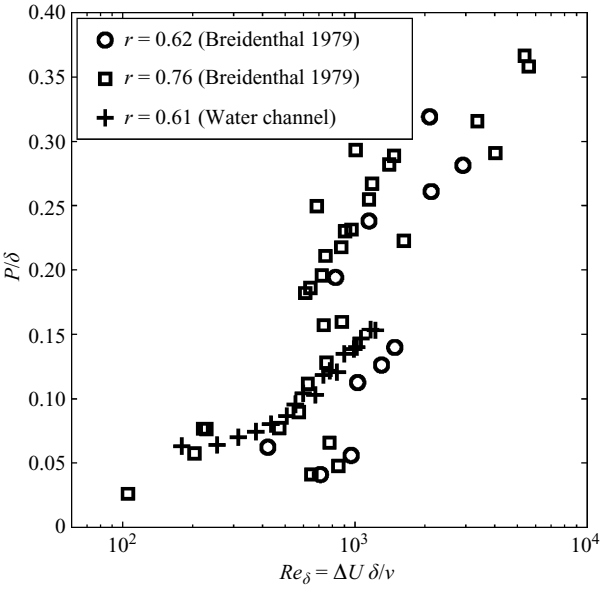

FIGURE 9. Equivalent chemical product thickness, P/δ, for the case of a liquid-phase, turbulent shear layer.

$Re_\delta > 8000$ observed by Breidenthal (1979) could not be reproduced in the channel; however, over the range of comparable Reynolds numbers shown in figure 9, the measurements of P/δ are within the scatter of Breidenthal's (1979) results for comparable velocity ratios (0.61, 0.62 and 0.76).

A measurement of the relative product thickness for the RT case, denoted P/h, is shown in figure 10. This work adopts $Re_h = 0.35\sqrt{A\,g\,h^3}/\nu$ (Ramaprabhu & Andrews 2004), where the RT mixing layer width (based on 5 %–95 % volume fraction thresholds) is the length scale (effectively the visual width of the RT mixing layer), and the terminal velocity of the dominant bubble is the velocity scale. It is difficult to directly compare shear-driven mixing layers with buoyancy-driven mixing layers due to the difference in Reynolds number definitions. However, for comparison purposes in figure 10, the shear layer Reynolds numbers and product thicknesses have been defined using δ_{vis} instead of δ. For the shear layer cases in figure 10, it is evident that the Reynolds number at which a significant rise in P/δ_{vis} occurs is a function of the velocity ratio and is also expected to be a function of the initial conditions associated with the initial vorticity shed from the splitter plate (Breidenthal 1979). While the Reynolds number definitions and initial conditions are not completely equivalent for the buoyancy- and shear-driven cases, their comparison in figure 10 reveals that the buoyancy-driven case exhibits an increasing trend in P/h, indicative of the onset of turbulence and a mixing transition at Reynolds numbers similar to those in the shear-driven case. However, higher-Reynolds-number RT instability experiments are needed to determine if buoyancy-driven turbulent mixing is capable of producing larger quantities of chemical product and if P/h attains an asymptotic value. Extrapolation from the shear-driven experiments suggests that asymptotic behaviour of P/h may not be observed in RT mixing until $Re_h \approx 8000$–10000, necessitating a different experimental facility for investigating high-Reynolds-number $Sc \sim 10^3$ mixing.

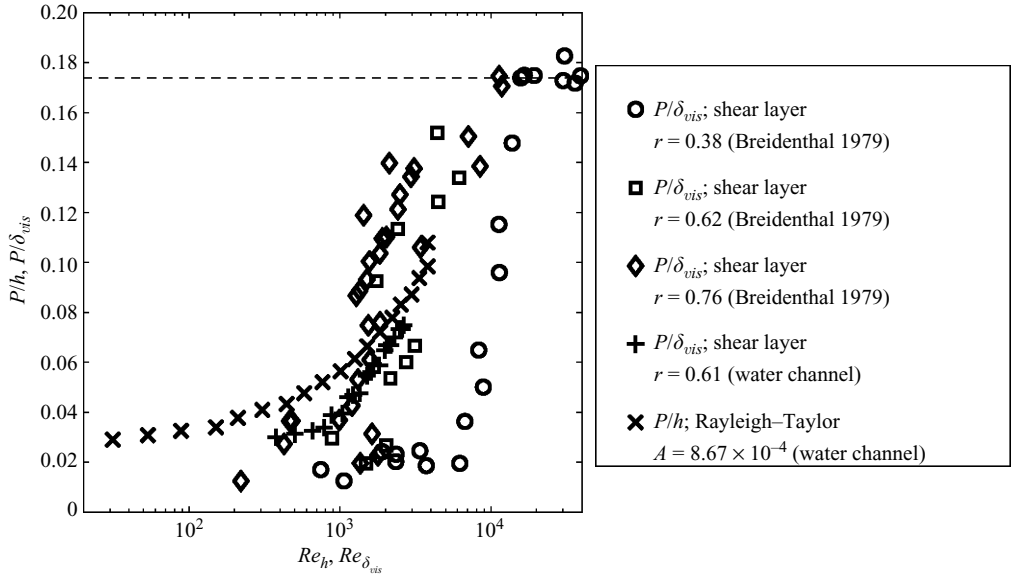

FIGURE 10. Equivalent product thickness for a liquid-phase RT mixing layer, P/h, and shear-driven mixing layer, P/δ_{vis}, at various velocity ratios r. The outer-scale Reynolds numbers are $Re_h = 0.35\sqrt{A\,g\,h^3}/\nu$ for the RT case and $Re_{\delta_{vis}} = \Delta U\,\delta_{vis}/\nu$ for the shear case. The asymptotic value $P/\delta_{vis} \approx 0.174$ for shear layers is also shown (dashed line).

4. Measurements of molecular mixing

The backlit optical technique described in § 2.2 provided measurements of the average concentration of coloured indicator $\overline{[\mathrm{In_{IV}}]}$, given two streams at $\mathrm{pH_1}$ and $\mathrm{pH_2}$. While these measurements of chemical product formation are a function of the degree of molecular mixing at small equivalence ratios, it is desirable to relate C to more conventional measures of molecular mixing. In this section, the measured passive scalar and reacting scalar concentration fields, $\bar{f}_1$ and C respectively, will be used to compute several parameters that quantify mixing.

4.1. *Measurements of product formation mixing parameter*

The measured indicator concentration profiles can be used to compute integral measures of the total quantity of chemical product formed, such as P/h. However, such a measure does not indicate the maximum quantity of chemical product that may be formed for the same equivalence ratio. Koochesfahani & Dimotakis (1986) quantified the degree of mixing in a reacting shear layer by normalizing the amount of product formed by the maximum product that could be formed if the two fluids homogeneously mixed. Cook & Dimotakis (2001) extended this concept to define an integral mixing parameter

$$\Xi(\phi_{\mathrm{In}}) = \frac{\int \overline{[\mathrm{In_{IV}}]}\,\mathrm{d}z}{\int \overline{[\mathrm{In_{IV}}]}_{max}\,\mathrm{d}z}, \tag{4.1}$$

where $\overline{[\mathrm{In_{IV}}]}_{max}$ is the maximum chemical product that could be produced if all fluid within the mixing layer were homogeneously mixed at a given equivalence ratio ϕ_{In}. This parameter is defined such that $\Xi = 0$ if no product is produced (i.e. the constituent fluids are completely segregated). Conversely, $\Xi = 1$ if all potential

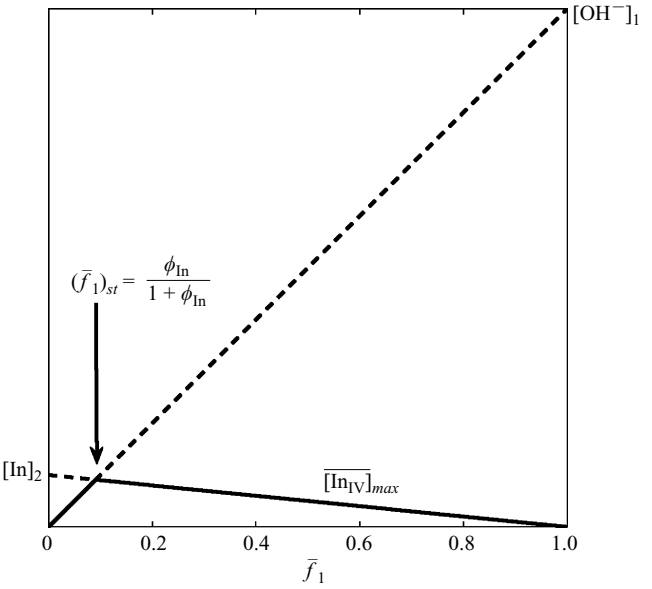

FIGURE 11. Schematic of maximum chemical product formation $\overline{[\mathrm{In_{IV}}]}_{max}$ (solid line) as a function of $\overline{f_1}$ and the equivalence ratio ϕ_{In}. The peak potential product formation occurs when the stoichiometric ratio of reactants are available at $(\overline{f}_1)_{st} = \phi_{\mathrm{In}}/(1+\phi_{\mathrm{In}})$.

product has been produced (i.e. the mixing layer is homogeneously mixed). For the two-fluid case (where $\bar{f}_1 + \bar{f}_2 = 1$) $\overline{[\mathrm{In_{IV}}]}_{max}$ depends upon the lean reactant such that

$$\overline{[\mathrm{In_{IV}}]}_{max} = \begin{cases} \bar{f}_1\,[\mathrm{OH^-}]_1, & \bar{f}_1 \leqslant (\bar{f}_1)_{st}, \\ (1-\bar{f}_1)\,[\mathrm{In}]_2, & \bar{f}_1 > (\bar{f}_1)_{st}, \end{cases} \tag{4.2}$$

where

$$(\bar{f}_1)_{st} = \frac{\phi_{\mathrm{In}}}{1+\phi_{\mathrm{In}}} \tag{4.3}$$

is the stoichiometric volume fraction of fluid 1 required to achieve a stoichiometric reaction; i.e. all reactants in (2.4) are entirely consumed. An illustration of the maximum product produced for a given equivalence ratio is shown in figure 11. The global mixing parameter Ξ is shown in figure 18, where it is compared with the global mixing parameter Θ defined in § 4.3.

4.2. *Use of chemical product formation measurements to quantify the degree of molecular mixing*

A useful measure of the degree of molecular mixing is given by the molecular mixing parameter

$$\theta = 1 - \frac{\sigma_{f_1}^2}{\bar{f}_1 \bar{f}_2}, \tag{4.4}$$

where $\sigma_{f_1}^2 = \overline{f_1'^2} = \overline{f_2'^2}$ is the volume fraction variance. As $0 \leqslant \sigma_{f_1}^2 \leqslant \bar{f}_1\bar{f}_2$, θ lies in the range 0–1. If the two fluids are completely unmixed (i.e. immiscible fluids) $\theta = 0$, and if the two fluids are uniformly molecularly mixed $\theta = 1$. This parameter has been reported by various researchers (Youngs 1994; Dalziel, Linden & Youngs 1999; Wilson & Andrews 2002; Ramaprabhu & Andrews 2004; Ristorcelli & Clark

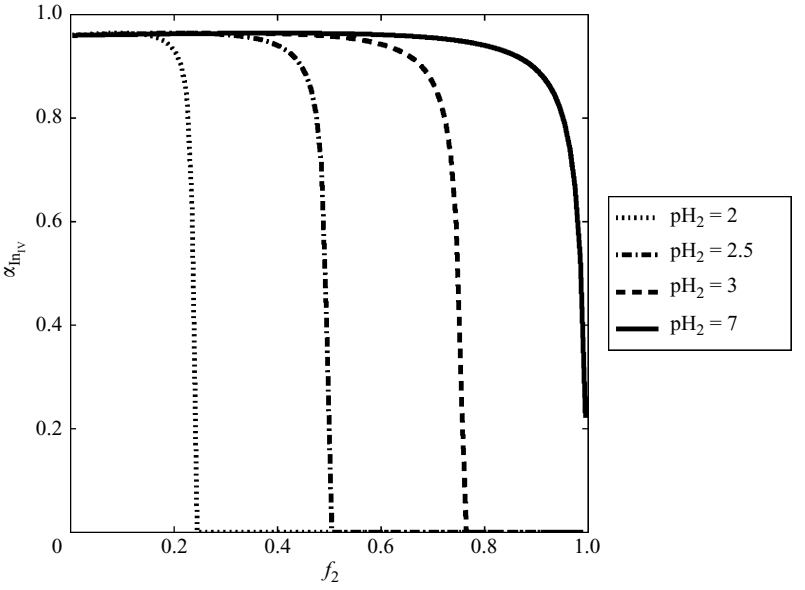

FIGURE 12. Fraction of dissociation for In_{IV} as a function of the volume fraction f_2 and pH_2 of the acidic stream.

2004; Mueschke *et al.* 2006) and provides a practical measure of molecular mixing, as transport equations for $\bar{f}_1$ and $\overline{f_1'^2}$ can be derived, modelled and solved to predict mixing (Chassaing *et al.* 2002; Veynante & Vervisch 2002; Fox 2003).

An approximation of the molecular mixing parameter can be obtained by measuring the amount of coloured product for a range of equivalence ratios. At a given point within the RT mixing layer, the probability of finding a given fraction by volume of fluid r is quantified by the p.d.f. $P(f_r)$. As noted earlier, fluid 1 is the heavier fluid with $pH_1 > 7$ (alkali), and fluid 2 is the lighter fluid with $pH_2 \leqslant 7$ (acidic or neutral) with a dilute amount of phenolphthalein added. Accordingly, the average concentration of indicator present within the mixing layer depends upon the indicator concentration in the lighter fluid (bottom stream) $[\mathrm{In}]_2$ and $\bar{f}_2$, the first moment of $P(f_2)$,

$$\overline{[\mathrm{In}]} = [\mathrm{In}]_2 \int_0^1 f_2\, P(f_2)\, \mathrm{d}f_2. \tag{4.5}$$

The total amount of indicator that is in its coloured form also depends on the fraction of dissociation $\alpha_{In_{IV}}$ (see (2.12)). This depends on the pH of the mixture, which in turn depends on pH_1, pH_2 and f_2. A modification to (4.5) gives the concentration of coloured indicator,

$$\overline{[\mathrm{In}_{IV}]} = [\mathrm{In}]_2 \int_0^1 \alpha_{In_{IV}}(\mathrm{pH})\, f_2\, P(f_2)\, \mathrm{d}f_2, \tag{4.6}$$

from which $C = \overline{[\mathrm{In}_{IV}]}/[\mathrm{In}]_2$ may then be evaluated. A simplification to (4.6) is made to estimate the molecular mixing parameter. If pH_1 is sufficiently large ($pH_1 \approx 11.5$ here), there is a relatively abrupt colour change as progressively more of fluid 1 is mixed with fluid 2. This is shown in figure 12 in which $pH_1 = 11.5$ is fixed and $\alpha_{In_{IV}}(f_2, pH_2)$ is plotted as a function of the volume fraction f_2 for various values of

pH_2. The fraction of dissociation is then approximated by a step function

$$\alpha_{\mathrm{In_{IV}}}\left(f_2, f_2^{50\%}\right) = \begin{cases} \alpha_{\mathrm{In_{IV}}}^{max} = 0.96, & f_2 \leqslant f_2^{50\%}, \\ 0, & f_2 > f_2^{50\%}, \end{cases} \tag{4.7}$$

where $f_2^{50\%}$ is the value of f_2 for which half of the indicator exists in its coloured form, i.e. $\alpha_{\mathrm{In_{IV}}} = 0.5$. This occurs when the mixture pH is 9.53. Note that $\alpha_{\mathrm{In_{IV}}}^{max} = 0.96$ because $\alpha_{\mathrm{In_{IV}}}$ does not attain unity for the maximum pH value of 11.5.

Substituting (4.7) into (4.6) allows the integral to be split into two parts and simplified:

$$\begin{aligned} C\left(f_2^{50\%}\right) &= \int_0^{f_2^{50\%}} \alpha_{\mathrm{In_{IV}}}\left(f_2, f_2^{50\%}\right) f_2\, P(f_2)\, \mathrm{d}f_2 + \int_{f_2^{50\%}}^1 \alpha_{\mathrm{In_{IV}}}\left(f_2, f_2^{50\%}\right) f_2\, P(f_2)\, \mathrm{d}f_2 \\ &= \alpha_{\mathrm{In_{IV}}}^{max} \int_0^{f_2^{50\%}} f_2\, P(f_2)\, \mathrm{d}f_2. \end{aligned} \tag{4.8}$$

Integrating over all values of $f_2^{50\%}$ gives

$$\frac{1}{\alpha_{\mathrm{In_{IV}}}^{max}} \int_0^1 C\left(f_2^{50\%}\right) \mathrm{d}f_2^{50\%} = \int_0^1 \left\{ \int_0^{f_2^{50\%}} f_2\, P(f_2)\, \mathrm{d}f_2 \right\} \mathrm{d}f_2^{50\%}. \tag{4.9}$$

Changing the order of integration on the right-hand side gives

$$\begin{aligned} \frac{1}{\alpha_{\mathrm{In_{IV}}}^{max}} \int_0^1 C\left(f_2^{50\%}\right) \mathrm{d}f_2^{50\%} &= \int_0^1 \left\{ \int_{f_2}^1 f_2\, P(f_2)\, \mathrm{d}f_2^{50\%} \right\} \mathrm{d}f_2 \\ &= \int_0^1 f_2\, P(f_2) \left\{ f_2^{50\%} \big|_{f_2}^1 \right\} \mathrm{d}f_2 \\ &= \int_0^1 (1 - f_2)\, f_2\, P(f_2)\, \mathrm{d}f_2 \\ &= \bar{f}_2 - \overline{f_2^2} = \bar{f}_2 - (\bar{f}_2)^2 - \sigma^2 = \bar{f}_1 \bar{f}_2 - \sigma^2. \end{aligned} \tag{4.10}$$

Hence the degree of molecular mixing becomes

$$\theta = 1 - \frac{\overline{f_1'^2}}{\bar{f}_1 \bar{f}_2} = \frac{\displaystyle\int_0^1 C\left(f_2^{50\%}\right) df_2^{50\%}}{\alpha_{\mathrm{In_{IV}}}^{max}\, \bar{f}_1 \bar{f}_2}. \tag{4.11}$$

At the centre plane of the mixing layer, $\bar{f}_1 = \bar{f}_2 = 1/2$, and θ further reduces to

$$\theta = \frac{4}{\alpha_{\mathrm{In_{IV}}}^{max}} \int_0^1 C\left(f_2^{50\%}\right) \mathrm{d}f_2^{50\%}. \tag{4.12}$$

The amount of coloured product has been measured for $pH_2 = 7.02$, 2.99, 2.44 and 2.02 while keeping $pH_1 \approx 11.5$, with corresponding values for $f_2^{50\%} =$ 0.986, 0.7583, 0.471 and 0.2411, respectively. For highly acidic streams, $pH_2 \to 1$ or $f_2^{50\%} \to 0$, and thus, no chemical indicator will exist in its coloured form, i.e. $C(f_2^{50\%} = 0) = 0$. Hence, five values of $C(f_2^{50\%})$ are shown for various evolution times (downstream locations) at the centreline in figure 13(*a*) and cross-stream locations in figure 13(*b*) at $\tau = 1$, using the chemical product measurements of figure 7. It is argued here that, as C must be a smoothly increasing function of $f_2^{50\%}$ with downstream distance, these data

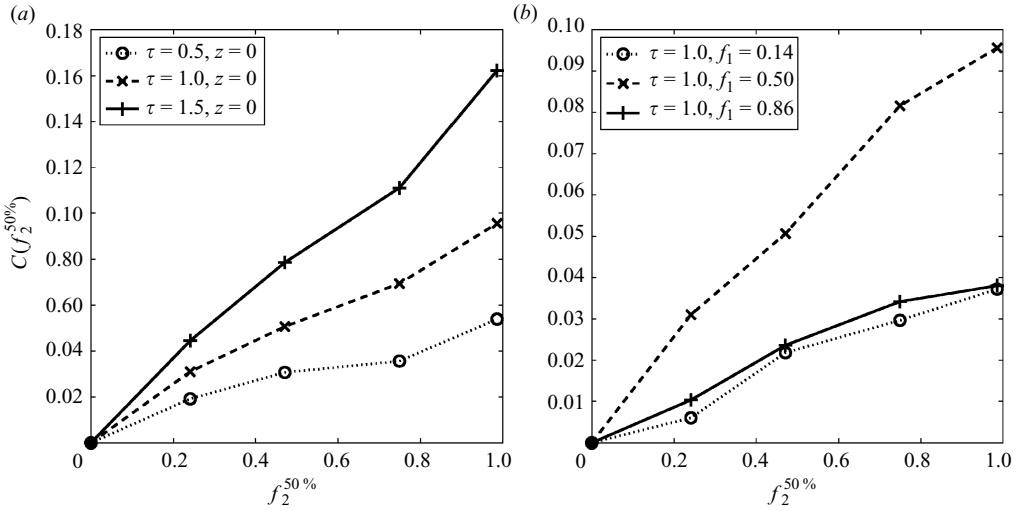

FIGURE 13. Measured values of coloured indicator concentration C for various pH_1/pH_2 combinations. Data for values ($f_2^{50\%}$, pH_1, pH_2) of (0.2411, 11.47, 2.02), (0.471, 11.52, 2.44), (0.7583, 11.53, 2.99) and (0.986, 11.48, 7.02) are shown. (*a*) Chemical product concentration measurements on the centre plane of the mixing layer at five different downstream locations. (*b*) Chemical product concentration measurements at five different positions across the mixing layer for a downstream location of $\tau = 1.0$.

points provide an adequate estimate of the integral (4.12). The simplest estimate for the integral (4.12) was obtained using a quadratic fit to the five data points. Similarly the cross-stream profiles in figure 13 correctly show a decrease in concentration away from the centreline, and the expected symmetry associated with off-centreline values at $f_1 = 0.14$ and 0.86 is reasonably satisfied.

4.3. *Measurement of molecular mixing parameters*

The terms on the right-hand side of (4.12), which include mean volume fraction and mean chemical indicator product profiles, were measured and are shown in figures 5, 7 and 13. Combining these measured concentration profiles according to (4.12) provides a measure of the volume fraction variance profiles shown in figure 14 across the RT mixing layer from $\bar{f}_1 = 0.1$ to $\bar{f}_1 = 0.9$. The 10 %–90 % volume fraction boundaries were used because measurements near the edges of the RT mixing layer are not converged due to a high degree of intermittency. The profiles in figure 14 are approximately parabolic with peaks at the centre plane of the mixing layer. The magnitude of $\overline{f_1'^2}$ on the centre plane ($z = 0$) has bounding values of 0 (perfectly mixed) and 0.25 (perfectly segregated). As the RT mixing layer grows, $\overline{f_1'^2}(z = 0)$ decreases in time, moving away from the immiscible limiting value of 0.25, indicating that a greater quantity of mixed fluid exists at later times.

The profiles of $\overline{f_1'^2}$ alone do not quantify the relative degree of molecular mixing, but such a measure is given by θ. To obtain profiles of θ, the volume fraction fluctuations (shown in figure 14) are combined with the mean volume fraction profiles (shown in figure 5) according to (4.12). Profiles of θ across the RT mixing layer are shown in figure 15 plotted between the 10 %–90 % volume fraction thresholds. For the small-Atwood-number case considered here, the profiles of θ are expected to be approximately constant across the RT mixing layer, as found in experiments (Wilson & Andrews 2002) and in numerical simulations (Youngs 1994; Ristorcelli & Clark

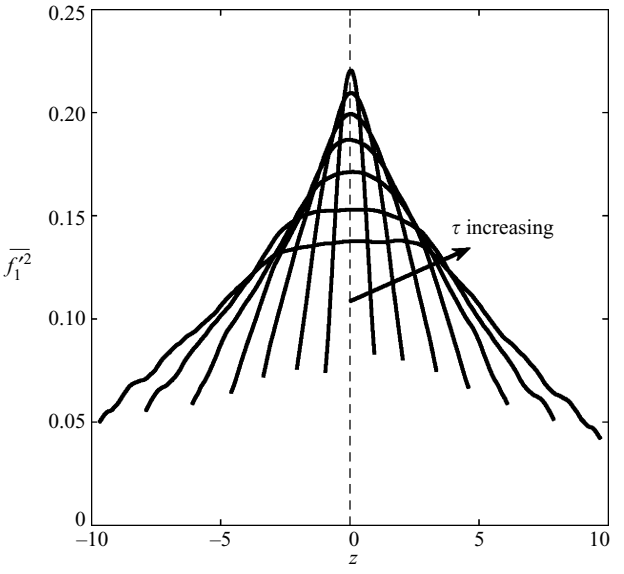

FIGURE 14. Profiles of $\overline{f_1'^2}$ across the mixing layer at dimensionless times $\tau = 0.25$, 0.50, 0.75, 1.00, 1.25, 1.50 and 1.75.

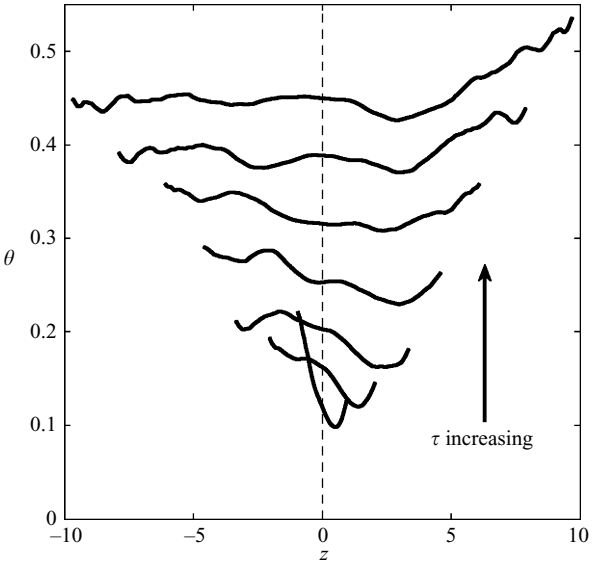

FIGURE 15. Profiles of θ across the mixing layer at dimensionless times $\tau = 0.25$, 0.50, 0.75, 1.00, 1.25, 1.50 and 1.75.

2004). If oscillations near the boundaries of the mixing layer are neglected because of increased uncertainty due to intermittency effects away from the centre plane, then the measured profiles of θ in figure 15 are reasonably constant at later times across the RT mixing layer in agreement with previous results.

Uncertainties in $\overline{f_1'^2}$ and θ are given by a combination of the uncertainties in the mean volume fraction measurement and indicator concentration measurements. Uncertainties in the mean nigrosine dye concentration measurements (as a result of (2.18)) contribute to uncertainties in the measured profiles of $\bar{f}_1$ and $\bar{f}_2$. Similarly,

τ	θ	w_θ/θ	w_θ
0.25	0.12	0.1787	0.021444
0.50	0.1639	0.1148	0.018816
0.75	0.2029	0.07392	0.014998
1.0	0.2529	0.05452	0.013788
1.25	0.3156	0.04175	0.013176
1.50	0.3886	0.03882	0.015085
1.75	0.4498	0.034378	0.015463

TABLE 2. Centreline uncertainty measurements for θ.

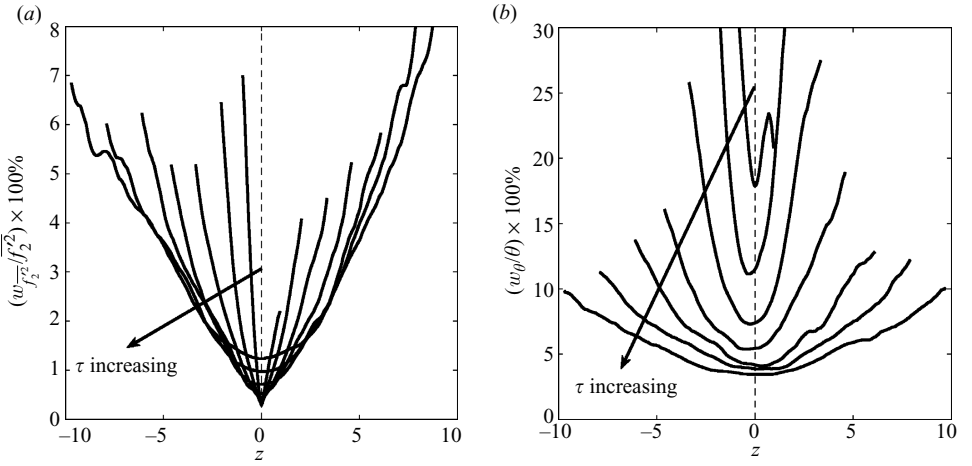

FIGURE 16. Relative uncertainties in the (*a*) $\overline{f_1'^2}$ and (*b*) θ profiles at dimensionless times $\tau = 0.25$, 0.50, 0.75, 1.00, 1.25, 1.50 and 1.75.

uncertainties in the mean chemical indicator concentration profiles contribute to uncertainties in the integral of (4.11). Figure 16(*a*) shows that when combined, the relative uncertainty in $\overline{f_1'^2}$ is less than $\pm 5\,\%$ within the mixing layer core. However, the statistical uncertainty in the $\overline{f_1'^2}$ measurements increases near the mixing layer boundaries due to a greater degree of intermittency. Combining the uncertainties in the mean and fluctuating volume fraction statistics gives a relative measure of the uncertainty in the measurement of θ. Table 2 shows that the absolute uncertainty in θ remains relatively unchanged at $w_\theta \approx \pm 0.015$ along the mixing layer centre plane for $0.1 < \tau < 1.9$. While this is a modest absolute uncertainty, as figure 16(*a*) shows, the relative uncertainty of approximately 20 % is large at early times due to the small values of θ. Away from the centre plane, the uncertainty estimate in θ increases to $w_\theta \approx \pm 0.05$.

Measurements of θ along the centre plane ($z = 0$) of the RT mixing layer were reported in previous water channel experiments (Wilson & Andrews 2002; Ramaprabhu & Andrews 2004; Mueschke *et al.* 2006) and in gas channel experiments (Kraft *et al.* 2009). The current centre plane measurements of θ are plotted in figure 17 with measurements from the gas channel in which $Sc = 0.7$ (Kraft *et al.* 2009) and the water channel for the hot/cold water case in which $Pr \equiv Sc = 7$ (Mueschke *et al.* 2006). Inspection of figure 17 reveals that a factor of 10 difference in Schmidt/Prandtl numbers (0.7 to 7) between the water and gas channel experiments gives a small difference in θ over $0.5 < \tau < 1.5$. However, comparison of the moderate

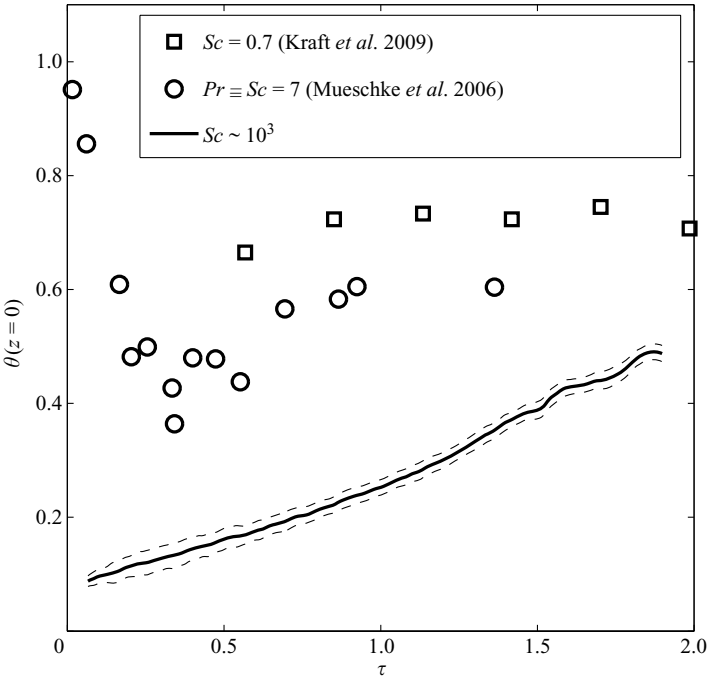

FIGURE 17. Evolution of θ on the centre plane of the mixing layer for various Schmidt numbers. Uncertainty bounds for the $Sc \sim 10^3$ measurements are indicated by the dashed lines. Measurements for the $Sc = 0.7$ case are taken from Kraft *et al.* (2009), and measurements for $Pr \equiv Sc = 7$ case are taken from Mueschke *et al.* (2006).

Schmidt number $Sc \sim 1$ measurements with the new $Sc \sim 10^3$ measurements shows a much larger and distinct difference. In particular, the minimum value of $\theta \approx 0.4$ was measured in the hot/cold water experiments at $\tau = 0.4$ before the RT mixing layer had transitioned to a fully three-dimensional, turbulent mixing layer. A similar value of $\theta \approx 0.4$ was only measured in the salt/fresh water experiments when the RT mixing layer reached $Re_h \approx 2000$ at $\tau = 1.5$. At the latest time measured ($\tau = 1.9$) $\theta \approx 0.5$, which begins to approach the late-time values measured in $Sc = 7$ water channel experiments. Thus, the present RT measurements are similar to the shear layer results (Konrad 1977; Breidenthal 1979, 1981), indicating that the Schmidt number has a smaller effect on the degree of molecular mixing at higher Reynolds numbers.

Youngs (1994) introduced a global molecular mixing parameter

$$\Theta = \frac{\int \overline{f_1 f_2}\,\mathrm{d}z}{\int \bar{f}_1 \bar{f}_2\,\mathrm{d}z} = 1 - \frac{\int \overline{f_1''^2}\,\mathrm{d}z}{\int \bar{f}_1 \bar{f}_2\,\mathrm{d}z} \tag{4.13}$$

analogous to the mixing parameter Ξ defined in § 4.1. As for θ and Ξ, $\Theta = 0$ when the two fluids are completely segregated, and $\Theta = 1$ when the two fluids are perfectly mixed. The mixing progress variables $\Xi(\phi_{\mathrm{In}} \to 0)$ and Θ were obtained from the present salt/fresh water experiments by integrating across the 10 %–90 % volume fraction thresholds. The evolution of Ξ and Θ is shown in figure 18. For times $\tau < 0.4$, $\Xi < 0.06$ and $\Theta < 0.15$, indicating that the majority of the fluid within the RT mixing layer exists as pockets of pure fluid that are stirred but not molecularly mixed. Just as with the evolution of θ shown in figure 17, both parameters increase

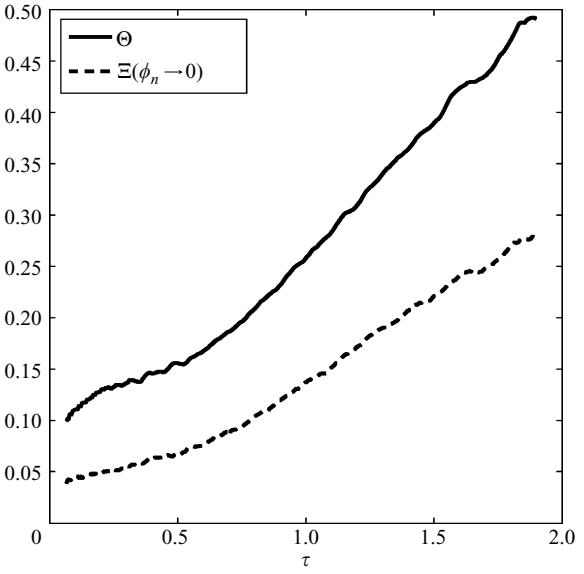

FIGURE 18. Evolution of the global mixing parameters Θ and Ξ for the $Sc \sim 10^3$ case.

and attain late-time values $\Xi \approx 0.28$ and $\Theta \approx 0.5$, although neither appears to attain an asymptotic value by $\tau = 1.9$. In comparison, Ramaprabhu, Dimonte & Andrews (2005) reported late-time values $\Theta \approx 0.7$–0.8, where monotone-integrated large-eddy simulations (MILES) were used to examine the influence of initial conditions on molecular mixing. Using a large-eddy simulation (LES), Cook, Cabot & Miller (2004) obtained $\Theta \approx 0.78$ for a moderate Atwood number ($A = 0.5$), $Sc = 1$ RT mixing layer. Thus, it is unclear whether θ or Θ in the $Sc \sim 10^3$ case reach the same asymptotic values measured in $Sc \sim 1$ experiments and simulations.

As shown in figure 10, the relative fraction of chemical product formed remains small until the onset of a fully turbulent regime at sufficiently high Reynolds numbers. This effect can be seen clearly in figure 18, where a transition in the slopes of Θ and Ξ occurs at $\tau \approx 0.5$. Before this transition both Θ and Ξ exhibit shallow, approximately linear slopes. Following this transition ($\tau > 0.5$), the slopes of Θ and Ξ increase, indicating that the production rate of mixed fluid has increased. The weak Reynolds number effect before $\tau \approx 0.5$ is because the RT mixing layer contains little three-dimensional structure and is in a weakly nonlinear regime. However, as the bandwidths of velocity and spatial scales increase, stretching of the interface between the two fluids increases both the surface area and concentration gradients driving molecular diffusion. This Reynolds number effect on θ, Θ and Ξ is shown more clearly in figure 19. As functions of Re_h, it is evident that the centre plane evolution of θ also exhibits the transition in slope at $\tau \approx 0.5$, corresponding to an integral-scale Reynolds number $Re_h \approx 300$.

As seen in the shear layer results of Konrad (1977) and Breidenthal (1979, 1981), a second transition is expected in the large-Reynolds-number limit, when each mixing parameter is expected to asymptote. Ristorcelli & Clark (2004) observed that the centre plane value of $\overline{f_1'^2}$ (and as a result θ) must be constant under the assumption of self-similarity. Approximately asymptotic behaviour in θ at the centre plane was observed in $Sc = 0.7$ gas-phase experiments (Kraft *et al.* 2009) and in $Pr = 7$ liquid-phase experiments (Mueschke *et al.* 2006). Dalziel *et al.* (1999) used

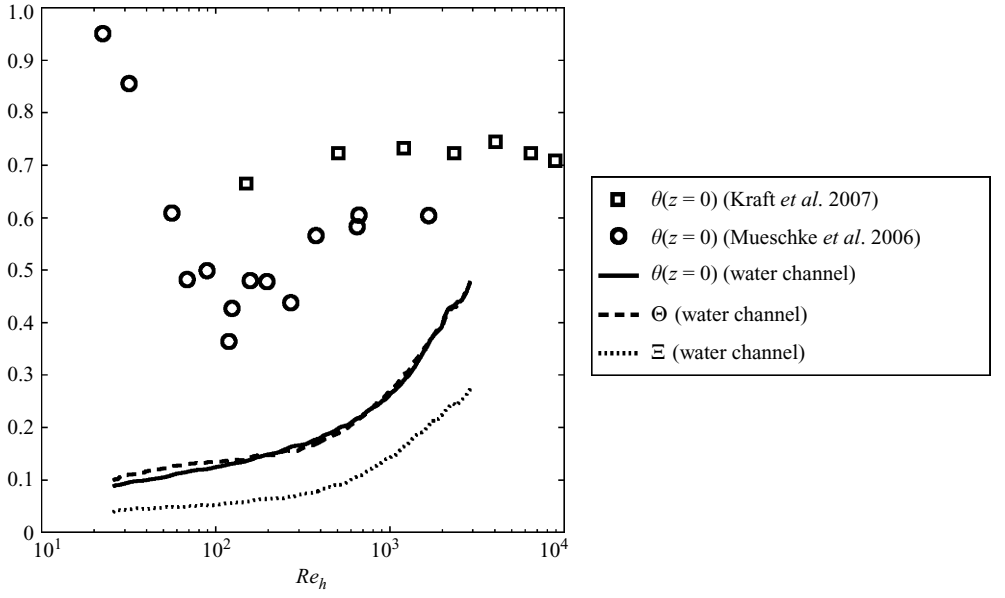

FIGURE 19. Evolution of mixing parameters as a function of the Reynolds number $Re_h = 0.35\sqrt{A\,g\,h^3}/\nu$.

light-induced fluorescence in a set of retracting plate experiments in a $Sc \sim 10^3$ salt/fresh water experiment and measured an approximately constant value $\Theta \approx 0.55$ over the range $0.4 < \tau < 1.5$ (when scaled to match the time normalization used in this work). However, their light-induced fluorescence measurements are not resolution-independent. The Batchelor scale for the analogous salt/fresh water experiments reaches $\eta_B = h\,Sc^{-1/2}Re^{-3/4} \approx 20\,\mu$m, and thus, under-resolved pointwise concentration measurements over-predict the degree of molecular mixing (Mueschke & Andrews 2005*a*, *b*). In the present work, where the measurement technique is free of optical resolution constraints, no asymptotic behaviour of the mixing parameters is observed by the largest Reynolds numbers achieved, $Re_h \approx 3000$. From figure 10, if buoyancy-driven mixing layers have an asymptotic value of P/h similar to that in shears layers, then an asymptotic behaviour of θ and Θ in the $Sc \sim 10^3$ mixing layers may not be observed until $Re_h \approx$ 8000–10 000.

5. Implications for turbulent transport and mixing modelling

Models of buoyancy-driven turbulent transport and mixing are designed to predict large-scale observables, such as the mixing layer width h and its late-time growth parameter α. To predict the relative degree of mixing, such models must also accurately predict second-order turbulence statistics, including the turbulent kinetic energy and density variance. These quantities have been an important subject of study in the reacting and combustion flow communities (Fox 2003; Poinsot & Veynante 2005) but have thus far received little attention in the RT community. Anisotropy effects, statistical inhomogeneity and non-equilibrium physics in RT mixing layers also complicate modelling. Predictive models must also encompass a large dynamic Reynolds number range. As shown in figure 19, models must capture the small mixing rate (shallow slope of θ and Θ) at $Re_h < 300$. At higher Reynolds numbers, models

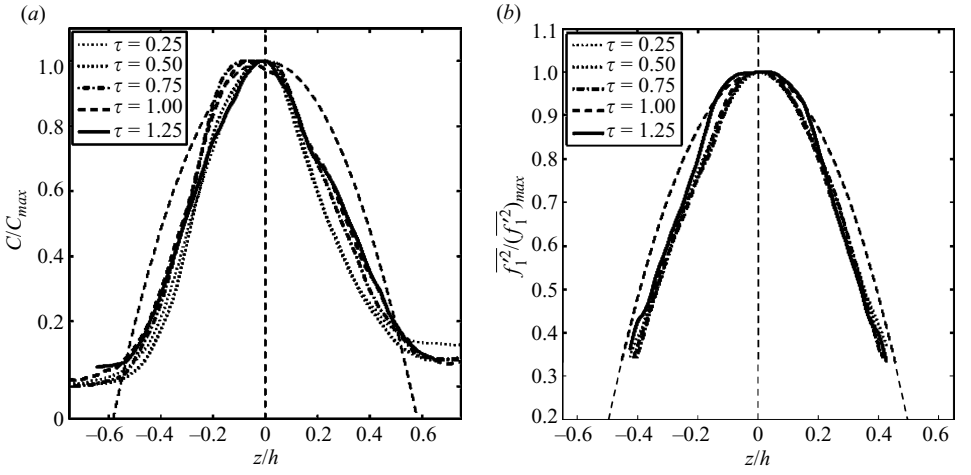

FIGURE 20. Self-similar collapse of (*a*) the coloured indicator concentration and (*b*) the volume fraction variance profiles. Parabolic profiles are shown as a reference (dotted line).

must account for an increased mixing rate, the expected self-similar collapse of the volume fraction variance profiles shown in figure 20 and the eventual asymptotic behaviour of P/h, θ and Θ. This suggests that the closures of the production and dissipation terms in the modelled density variance $\overline{\rho'^2}$ (or equivalently $\overline{f_1'^2}$) transport equation may strongly depend on an integral-scale Reynolds number Re_h or a turbulent Reynolds number $Re_t = K^2/(\nu\varepsilon)$, where K and ε are the turbulent kinetic energy and its dissipation rate, respectively. Liu & Fox (2006) addressed this issue by analytically integrating model scalar spectra to determine the relationship between the mechanical and scalar time scales as a function of Re_t and Sc. However, the model proposed by Liu & Fox (2006) implies that the integral length scale is set by the bounding geometry (rather than the flow), which is not the case for RT instability-driven mixing. In addition, the model kinetic energy and scalar variance spectra neglect spectral non-equilibrium effects (Pope 2000; Fox 2003). Thus, the dependence of the mixing rate on the initial perturbations at the fluid interface cannot be incorporated, which has been shown to have persisting effects to at least $Re_h > 10^3$ (Cook & Dimotakis 2001, 2002; Ramaprabhu *et al.* 2005; Mueschke *et al.* 2006).

A complete specification of transport models for high-Schmidt-number RT mixing requires measurements of transport quantities such as $\overline{f_1}$ and $\overline{f_1'^2}$. However, there is currently little detailed data available from direct numerical simulations (DNSs) and experiments (compared with shear-driven turbulence) to aid in the validation of such models for RT instability-driven mixing. While DNS of RT driven mixing are available at $Sc = 1$ (Cook & Dimotakis 2001, 2002; Ristorcelli & Clark 2004; Cabot & Cook 2006), no such data is available for the large-Schmidt-number case, for which DNS is too computationally expensive. In addition, there are few subgrid-scale models suitable for LES of large-Schmidt-number mixing (Pullin 2000; Burton 2008). Furthermore, MILES and implicit large-eddy simulation (ILES) do not include molecular dissipation and diffusion terms (having a numerical Schmidt number $O(1)$) and are thus poorly suited to investigating Schmidt number effects on molecular

mixing. Thus, the experimental results of the present work provide the sole data for assessing transport models for high-Schmidt-number RT mixing.

6. Conclusions

Experiments measuring the degree of molecular mixing in a liquid-phase, high-Schmidt-number RT instability-driven mixing layer have been performed using a salt/fresh water configuration in a water channel. The measured RT mixing layer growth parameter $\alpha = 0.085 \pm 0.005$ for this salt/fresh water case indicates that the Schmidt number may have a minor influence on the late-time self-similar growth of the RT mixing layer. To quantify the degree of molecular mixing, the pH of each water stream was altered, and a diffusion-limited neutralization reaction was monitored by the addition of a pH-sensitive chemical indicator. For the limiting case of the equivalence ratio $\phi_{\mathrm{In}} \rightarrow 0$, the chemical indicator concentration profiles indicate the degree of molecular mixing between the two fluids. As the buoyancy-driven mixing developed, the quantity of chemical indicator measured continued to increase, showing that the quantity of mixed fluid within the turbulent core of the RT mixing layer increased with Reynolds number. Novel measurements of equivalent product thickness were reported, where P/h continues to increase with Reynolds number at late times. The onset of a turbulent transition at $Re_h \approx Re_{\delta_{vis}} > 10^3$ was demonstrated by the increased rate of chemical product formation. However, the final mixing transition stage indicated by an asymptotic value of P/h, as seen in high-Reynolds-number shear flows, was not observed for $Re_h \leqslant 3000$.

New measurements of the degree of molecular mixing were reported using both the relative fraction of chemical product formed and fluctuating density statistics. Relationships between the measured mean passive scalar profiles, chemical indicator concentration profiles and the density variance were developed. The first measurements of volume fraction variance profiles $\overline{f_1'^2}$ for $Sc \sim 10^3$ RT mixing were obtained by integrating the total indicator formation over the range of equivalence ratios $0 < \phi_n < \infty$ (or $0 < f_2^{50\,\%} < 1$). These profiles are approximately parabolic, and the peak magnitude decreases in time, indicating a greater volume of mixed fluid at later times. Combining measurements of $\bar{f}_1$ and $\overline{f_1'^2}$, a resolution-independent measurement of the molecular mixing parameter θ was obtained for the $Sc \sim 10^3$ case and was compared with lower-Schmidt-number (0.7 and 7) experimental measurements. It was found that the larger Schmidt number in the salt/fresh water experiments resulted in a significant decrease in θ for all times measured. In addition to the local mixing parameter θ, measurements of the global mixing parameters Ξ and Θ were also reported. Similar to θ, both Ξ and Θ were significantly lower than any values reported for $Sc \sim 1$ experiments and simulations. All parameters indicate an initial transition to a turbulent regime at $\tau \approx 0.5$ or $Re_h \approx 300$, where the initially shallow linear slope of each parameter begins to increase. At the latest time, all of the molecular mixing parameters increased. It remains unclear whether $Sc \sim 10^3$ RT mixing layers attain the same asymptotic value of θ as in lower-Schmidt-number RT mixing experiments.

This research was supported by the US Department of Energy National Nuclear Security Administration under the Stewardship Science Academic Alliances programme through DOE Research Grant #DE-FG03-02NA00060. This work was

also performed under the auspices of Lawrence Livermore National Laboratory under contract no. DE-AC52-07NA27344.

Appendix A. Neutralization chemistry

In aqueous solutions, the concentration of hydrogen and hydroxide ions satisfy the reversible reaction

$$H_2O \Leftrightarrow H^+ + OH^- \tag{A 1}$$

with equilibrium constant

$$K_w = [H^+]\,[OH^-] = 1 \times 10^{-14}. \tag{A 2}$$

A mixture of two fluids with volume fractions f_1, f_2 and hydrogen ion concentrations pH_1, pH_2 will reach a new equilibrium value pH_{mix} as determined by conservation of mass and equilibrium constraints. The initial, unmixed ion concentrations are given by

$$a_0 = f_1\,[H^+]_1 + f_2\,[H^+]_2, \tag{A 3}$$

$$b_0 = f_1\,[OH^-]_1 + f_2\,[OH^-]_2, \tag{A 4}$$

which may not necessarily satisfy the equilibrium constraint in (A2). Upon mixing, a_0 and b_0 will decrease by an amount x, giving final concentrations $a_{mix} = a_0 - x$ and $b_{mix} = b_0 - x$. The new equilibrium concentrations a_{mix} and b_{mix} must then satisfy the equilibrium constraint (A2), where

$$\begin{aligned} K_w &= [H^+]\,[OH^-] \\ &= (a_0 - x)(b_0 - x) \\ &= a_0 b_0 - x(a_0 + b_0) + x^2. \end{aligned} \tag{A 5}$$

The change in ion concentrations, x, can be calculated by solving the quadratic equation in (A5), giving

$$x = \frac{(a_0 + b_0) - \sqrt{(a_0 + b_0)^2 - 4(a_0 b_0 - K_w)}}{2}, \tag{A 6}$$

where the negative root provides the physical solution. Accordingly, the final pH of the mixture is given by $pH_{mix} = -\log_{10}(a_0 - x)$.

REFERENCES

Anuchina, N. N., Kucherenko, Y. A., Neuvazhaev, V. E., Ogibina, V. N., Shibarshov, L. I. & Yakovlev, V. G. 1978 Turbulent mixing at an accelerating interface between liquids of different densities. *Izv. Akad Nauk. SSSR, Mekh. Zhidk. Gaza* **6**, 157–160.

Atzeni, S. & Meyer-ter-Vehn, J. 2004 *The Physics of Inertial Fusion: Beam Plasma Interaction, Hydrodynamics, Hot Dense Matter*, International Series of Monographs on Physics, vol. 125. Oxford University Press.

Benedict, L. H. & Gould, R. D. 1996 Towards better uncertainty estimates for turbulence statistics. *Exp. Fluids* **22**, 129–136.

Betti, R., Umansky, M., Lobatchev, V., Goncharov, V. N. & McCrory, R. L. 2001 Hot-spot dynamics and deceleration-phase Rayleigh–Taylor instability of imploding inertial confinement fusion capsules. *Phys. Plasmas* **8**, 5257–5267.

Bishop, E. (Ed.) 1972 *Indicators*, International Series of Monographs in Analytical Chemistry. Pergamon.

Breidenthal, R. 1979 A chemically reacting turbulent shear layer. PhD dissertation, California Institute of Technology.

Breidenthal, R. 1981 Structure in turbulent mixing layers and wakes using a chemical reaction. *J. Fluid Mech.* **109**, 1–24.

Browand, F. K. & Weidman, P. D. 1976 Large scales in the developing mixing layer. *J. Fluid Mech.* **76**, 127–144.

Brown, G. L. & Roshko, A. 1974 On density effects and large structure in turbulent mixing layers. *J. Fluid Mech.* **64**, 775–816.

Burton, G. C. 2008 The nonlinear large-eddy simulation method applied to $Sc \approx 1$ and $Sc \gg 1$ passive-scalar mixing. *Phys. Fluids* **20**, 035103-1–035103-14.

Cabot, W. H. & Cook, A. W. 2006 Reynolds number effects on Rayleigh–Taylor instability with possible implications for type-Ia supernovae. *Nat. Phys.* **2**, 562–568.

Chandrasekhar, S. 1961 *Hydrodynamic and Hydromagnetic Stability*. Dover.

Chassaing, P., Antonia, R. A., Anselmet, F., Joly, L. & Sarkar, S. 2002 Variable Density Fluid Turbulence. In *Fluid Mechanics and Its Applications*, vol. 69. Kluwer Academic.

Cook, A. W., Cabot, W. & Miller, P. L. 2004 The mixing transition in Rayleigh–Taylor instability. *J. Fluid Mech.* **511**, 333–362.

Cook, A. W. & Dimotakis, P. E. 2001 Transition stages of Rayleigh–Taylor instability between miscible fluids. *J. Fluid Mech.* **443**, 69–99.

Cook, A. W. & Dimotakis, P. E. 2002 Corrigendum. *J. Fluid Mech.* **457**, 410–411.

Cui, A. Q. & Street, R. L. 2004 Large-eddy simulation of coastal upwelling flow. *Environ. Fluid Mech.* **4**, 197–223.

Dalziel, S. B., Linden, P. F. & Youngs, D. L. 1999 Self-similarity and internal structure of turbulence induced by Rayleigh–Taylor instability. *J. Fluid Mech.* **399**, 1–48.

Danckwerts, P. V. 1952 The definition and measurement of some characteristics of mixtures. *Appl. Sci. Res.* A **3**, 279–296.

Desai, M. A. & Vadgama, P. 1991 Estimation of effective diffusion coefficients of model solutes through gastric mucus: assessment of a diffusion chamber technique based on spectrophotometric analysis. *Analyst* **116**, 1113–1116.

Dimotakis, P. E. 2005 Turbulent mixing. *Annu. Rev. Fluid Mech.* **37**, 329–356.

Fox, R. O. 2003 *Computational Models for Turbulent Reacting Flows*. Cambridge University Press.

Green, F. J. 1990 *The Sigma-Aldrich Handbook of Stains, Dyes, and Indicators*. Aldrich Chemical Co.

Haan, S. W. 1989 Onset of nonlinear saturation for Rayleigh–Taylor growth in the presence of a full spectrum of modes. *Phys. Rev.* A **39**, 5812–5825.

Harris, D. C. 2003 *Quantitative Chemical Analysis*, 6th ed. W. H. Freeman.

Hecht, E. 2002 *Optics*, 4th ed. Addison Wesley.

Kolthoff, I. M. 1937 *Acid–Base Indicators*. Macmillan.

Konrad, J. H. 1977 An experimental investigation of mixing in two-dimensional turbulent shear flows with applications to diffusion-limited chemical reactions. PhD dissertation, California Institute of Technology.

Koochesfahani, M. M. & Dimotakis, P. E. 1986 Mixing and chemical reactions in a turbulent liquid mixing layer. *J. Fluid Mech.* **170**, 83–112.

Koop, G. K. 1976 Instability and turbulence in a stratified shear layer. PhD dissertation, University of Southern California.

Kraft, W., Banerjee, A. & Andrews, M. J. 2009 On hot-wire diagnostics in Rayleigh–Taylor mixing layers. *Exp. Fluids*. doi:10.1007/S00348-009-0636-3.

Kukulka, D. J. 1981 Thermodynamic and transport properties of pure and saline water. MS thesis, State University of New York at Buffalo.

Lide, D. R. (Ed.) 2006 *CRC Handbook of Chemistry and Physics*, 87th ed. CRC Press.

Linden, P. F. & Redondo, J. M. 1991 Molecular mixing in Rayleigh–Taylor instability. Part I. Global mixing. *Phys. Fluids* A **3**, 1269–1277.

Linden, P. F., Redondo, J. M. & Youngs, D. L. 1994 Molecular mixing in Rayleigh–Taylor instability. *J. Fluid Mech.* **265**, 97–124.

Lindl, J. D. 1998 *Inertial Confinement Fusion: The Quest for Ignition and Energy Gain Using Indirect Drive*. Springer.

Liu, Y. & Fox R. O. 2006 CFD predictions for chemical processing in a confined impinging-jets reactor. *AIChE J.* **52**, 731–744.

Marmottant, P. H. & Villermaux, E. 2004 On spray formation. *J. Fluid Mech.* **498**, 73–111.

Molchanov, O. A. 2004 On the origin of low- and middler-latitude ionospheric turbulence. *Phys. Chem. Earth* **29**, 559–567.

Mueschke, N. J. & Andrews, M. J. 2005*a* Investigation of scalar measurement error in diffusion and mixing processes. *Exp. Fluids* **40**, 165–175.

Mueschke, N. J. & Andrews, M. J. 2005*b* Erratum. *Exp. Fluids* **40**, 176.

Mueschke, N. J., Andrews, M. J. & Schilling, O. 2006 Experimental characterization of initial conditions and spatio-temporal evolution of a small-Atwood-number Rayleigh–Taylor mixing layer. *J. Fluid Mech.* **567**, 27–63.

Mungal, M. G. & Dimotakis, P. E. 1984 Mixing and combustion with low heat release in a turbulent shear layer. *J. Fluid Mech.* **148**, 349–382.

Poinsot, T. & Veynante, D. 2005 *Theoretical and Numerical Combustion*, 2nd ed. R. T. Edwards.

Pope, S. B. 2000 *Turbulent Flows*. Cambridge University Press.

Pullin, D. I. 2000 A vortex-based model for the subgrid flux of a passive scalar. *Phys. Fluids* **12**, 2311–2319.

Ramaprabhu, P. & Andrews, M. J. 2003 Simultaneous measurements of velocity and density in buoyancy-driven mixing. *Exp. Fluids*, **34**, 98–106.

Ramaprabhu, P. & Andrews, M. J. 2004 Experimental investigation of Rayleigh–Taylor mixing at small Atwood numbers. *J. Fluid Mech.* **502**, 233–271.

Ramaprabhu, P., Dimonte, G. & Andrews, M. J. 2005 A numerical study of the influence of initial perturbations on the turbulent Rayleigh–Taylor instability. *J. Fluid Mech.* **536**, 285–319.

Rayleigh, J. W. 1884 Investigation of the equilibrium of an incompressible heavy fluid of variable density. *Proc. Lond. Math. Soc.* **14**, 170–177.

Ristorcelli, J. R. & Clark, T. T. 2004 Rayleigh–Taylor turbulence: self-similar analysis and direct numerical simulations. *J. Fluid Mech.* **507**, 213–253.

Shea, J. R. 1977 A chemical reaction in a turbulent jet. *J. Fluid Mech.* **81**, 317–333.

Smarr, L., Wilson, J. R., Barton, R. T. & Bowers, R. L. 1981 Rayleigh–Taylor overturn in super nova core collapse. *Astrophys. J.* **246**, 515–525.

Snider, D. M. & Andrews, M. J. 1994 Rayleigh–Taylor and shear driven mixing with an unstable thermal stratification. *Phys. Fluids* A **6**, 3324–3334.

Stillinger, D. C., Head, M. J., Helland, K. N. & Van Atta, C. W. 1983 A closed loop gravity-driven water channel for density stratified shear flow. *J. Fluid Mech.* **131**, 73–89.

Taylor, G. I. 1950 The instability of liquid surfaces when accelerated in a direction perpendicular to their planes. *Proc. R. Soc. Lond.* **201**, 192–196.

Thomas, G. O. 2003 The aerodynamic breakup of ligaments. *Atom. Sprays* **13**, 117–129.

Veynante, D & Vervisch, L. 2002 Turbulent combustion modeling. *Prog. Energy Combust. Sci.* **28**, 193–266.

Warhaft, Z. 2000 Passive scalars in turbulent flows. *Annu. Rev. Fluid Mech.* **32**, 203–240.

Wilson, P. N. & Andrews, M. J. 2002 Spectral measurements of Rayleigh–Taylor mixing at low-Atwood number. *Phys. Fluids* A **14**, 938–945.

Youngs, D. L. 1984 Numerical simulations of turbulent mixing by Rayleigh–Taylor instability. *Physica* D **12**, 32–44.

Youngs, D. L. 1994 Numerical simulation of mixing by Rayleigh–Taylor and Richtmyer–Meshkov instabilities. *Laser Part. Beams* **12**, 725–750.

Zhang, S. & Schneider, S. P. 1995 Quantitative molecular-mixing measurements in a round jet with tabs. *Phys. Fluids* **7**, 1063–1070.

Zhang, S., Schneider, S. P. & Collicott, S. H. 1995 Quantitative molecular-mixing measurements using digital processing of absorption images. *Exp. Fluids* **19**, 319–327.